Chapter 2. EASTERN OCEAN BOUNDARIES
COASTAL SEGMENT (E)

A. EDWARD HILL

School of Ocean Sciences, University of Wales, Bangor

BARBARA M. HICKEY

School of Oceanography, University of Washington

FRANK A. SHILLINGTON

University of Cape Town

P. TED STRUB

College of Oceanic and Atmospheric Sciences, Oregon State University

KENNETH H. BRINK

Woods Hole Oceanographic Institution

ERIC D. BARTON

School of Ocean Sciences, University of Wales, Bangor

ANDREW C. THOMAS

School of Marine Sciences, University of Maine

Contents

The Sea, Volume 11, edited by Allan R. Robinson and Kenneth H. Brink
ISBN 0-471-11545-2

1. Introduction

Scientifically, our view of the ocean margins is changing subtly. Traditionally, we have approached them with questions relating to how the open ocean controls their dynamics (e.g., with regard to tidal phenomena on the shelf) or we have tended to treat the shelf in isolation from the deep ocean (e.g., when considering wind-driven currents). Increasingly, however, attention has turned to questions of ocean–shelf exchange and to how ocean margin processes influence the deep ocean through, for example, boundary mixing, downslope export of carbon and dense water formation. The discovery of surface filaments that penetrate 50–300 km offshore into the open ocean highlights one specific process of potential importance for offshore export off eastern boundaries.

The eastern boundaries of the world's oceans are notably productive, with four of the five major upwelling systems located on them. The coastal zone off Peru and Chile, for example, accounts for about 15% of the estimated 80 million tonnes of marine fish landed globally (FAO, 1992). Other important resources, such as minerals and hydrocarbons, are also exploited in these regions and eastern boundaries support major centers of human population. The nations situated on these boundaries range from some of the most prosperous to some of the poorest in the world, and the distribution and economic impact of eastern boundary resources vary immensely, as do the nature and extent of human impact on these environments.

Eastern boundary dynamics and phenomena are considered in this chapter. The review is not comprehensive and our more limited objectives are (1) to draw out those aspects where there is a high degree of commonality between regions, (2) to highlight particularly remarkable features, and (3) to identify goals for future research. To this end, one contribution of the chapter is to summarize in Table I the key aspects of the main eastern boundary subregions in a way that should enable the salient features of each to be appreciated and compared at a glance. Further details of the individual eastern boundary systems can be found in the complementary set of regional reviews (and the references therein) in Chapters 10 to 13, 20 to 23, 25, 27, and 33. Much of the dynamical background relevant to eastern boundaries is covered in the reviews by Brink (1997) and Huyer (1990).

In Section 2 the geographical setting of the main eastern boundary regions is described briefly. In Section 3 attention turns to an account of the major oceanographic phenomena found on eastern boundaries and the processes that establish them. The chapter concludes with a discussion of the major research goals that lie ahead.

2. Geographical Setting

The two principal meridional eastern boundaries are those on the margins of the Pacific Ocean (55°S–67°N) and the Atlantic Ocean (35°S–70°N) (Figure 2.1). The Indian Ocean eastern boundary has a lesser meridional extent and is more complex, made up in part from the Australian west coast and the Indonesian Archipelago (Fig. 2.1). The west coasts of India, Greenland and New Zealand are also eastern margins, although of more limited extent. Eastern boundaries encompass the entire range of climatic conditions found on earth from arctic to equatorial. Most eastern boundary continental shelves are relatively narrow (10–100 km wide) and the coastal orientation is predominantly meridional or has a strong meridional component. In several locations, however—the Gulf of Guinea (West Africa), the northern and southern coasts of Iberia (Europe), the Gulf of Alaska (North America) and southern Peru—the boundary orientation is zonal; the potential dynamical significance of this is mentioned later. While most eastern boundary continental shelves are narrow, three important exceptions are the northwest Australian Shelf (Chapter 33), the northwest European Shelf (Chapter 23), and the Bering Shelf (Chapter 27). The extensive Java Sea Shelf (Chapter 17) is probably best not classified as an eastern boundary shelf because it is located behind the island chain that constitutes the eastern boundary proper. The Northwest European and Bering Shelves, respectively, are located at the northern margins of the Atlantic and Pacific eastern boundaries; both are semienclosed, have dimensions of order 1000 km and are tidally energetic.

On the Pacific eastern boundary and in southern South Africa, landmasses take the form of high-altitude mountain ranges or plateaus, and at high latitudes the eastern boundary coastlines are fjordic. This has several important influences on the coastal forcing regimes. For example, the high-altitude boundary promotes the poleward propagation of coastally trapped atmospheric low-pressure systems in southwest Africa, the Pacific coast of North America and northern Chile (Chapters 10 and 20; Hermann et al., 1990). The significance of these propagating atmospheric systems is that they are the source of 3- to 10-day variability in the upwelling wind stress (e.g., off Chile), and off western South Africa it has been suggested that they are resonant with the oceanic coastal trapped waves. In Central America, high mountain ranges act as a barrier between the warm Pacific coastal airmass and the cold, winter, North American continental airmass which occasionally outbreaks over the Gulf of Mexico. Mountain passes funnel this air over the Pacific eastern margin as strong offshore wind jets in winter that have important local impacts on the coastal ocean discussed later (Chapter 11; Barton et al., 1993). High-altitude landmasses and often desertic conditions also mean that there are few well-developed river catchment systems on eastern boundaries, hence few large individual rivers (although there are exceptions such as the Columbia River, with a discharge of 7300 $m^3\ s^{-1}$ on the Pacific coast of North America, and the Bio Bio River in Chile, with a winter discharge of 1200 $m^3\ s^{-1}$). Large areas of the midlatitude eastern boundaries are situated in the arid or semiarid climate belt, but where precipitation is high in the temperate and subpolar regions, freshwater discharge often takes place in the form of numerous small streams (Chapter 13) or as brief but rare flood events such as off southwest Africa (Chapter 20). A notable exception to the generally high-altitude terrain is the low-lying eastern boundary of Equatorial West Africa (also high in precipitation), where the Zaire and Niger Rivers are major localized sources of freshwater buoyancy input. In northwest Europe, the semienclosed Baltic Sea acts as an integrator of numerous small river inputs from northern Europe and acts as a freshwater source for the Norwegian Coastal Current (Hill, 1997). Similarly the Strait of Juan de Fuca is an important freshwater source on the North Pacific eastern margin which produces the Vancouver Island Coastal Current (Thomson et al., 1990).

The local wind systems on eastern boundaries are controlled over large areas by subtropical atmospheric high-pressure (anticyclonic) systems in which airmasses descend in the Hadley–Walker atmospheric circulation cells leading to low precipitation. The result is a predominantly equatorward component of wind stress over the subtropical, arid coastal boundaries (Fig. 2.2). At the poleward margins of this zone

TABLE I
Summary of Eastern Boundary Phenomena and Processes[a]

	Southwest Africa (Benguela)	Equatorial West Africa	Northwest Africa	Strait of Gibraltar	Iberia	Biscay–French Shelf	NW European Shelf	Norway
Principal climatic influence	South Atlantic High, polar front storms	ITCZ, SE trades in Gulf of Guinea	Azores High	Azores High, Mediterranean	Azores High	Azores High, polar front depressions	Azores High, SE Iceland Low, polar front depressions	SE Iceland Low, atmospheric polar front
Principal oceanic influence	Agulhas rings, Angolan Current (P)	EUC, SACW	Canary Current (E), NACW/ SACW, NECC	Mediterranean Water, Atlantic Ocean	Portugal Current (E)		North Atlantic Current (P)	Norwegian Current (P)
Topography	Deep shelf break, smooth topography	Shelf <30 km wide canyons	Generally narrow shelf, wide in places	Strait and sill	Narrow shelf	Narrow shelf in south widening northwards	Wide shelf, slope with canyons in Celtic Sea	Norwegian Trench, fjordic coast
Winds	Strong equatorward	Steady, weak, SW	NE Trades		NE trades (summer)	Westerly, southwestly	Mean SW, storms	Frequent storms
Fresh water input	Arid, occasional summer flood events	2 m yr^{-1} rainfall, Zaire and Niger Rivers	None	None	Small, Spanish rias in north	Gironde Estuary	Irish Sea, English Channel, Rhine	From fjords and Baltic Sea outflow
Tides	Weak semidiurnal	Amplification of fortnight MS_f	Weak	Semidiurnal internal tides, solitons	Internal tide generations, solitons	Internal tide generation, solitons, shelf tides increase northward	Semidiurnal, macrotidal, internal tide generation and solitons on slope	Semidiurnal, with amphidromic systems along coast

Poleward flow	Bottom layer on shelf, shelf break	EUC divides and flows poleward along slope	Subsurface: 0.1 m s^{-1}, core at 300 m, <100 km wide	Dense Mediterranean plume flows poleward	Along shelf edge, turns 90° to flow along North Spanish slope	0.02–0.06 m s^{-1} increasing northward, weak on North Spanish slope	Celtic–Porcupine–Rockall slope current strengthening northward to 0.2 m s^{-1}	Norwegian coastal current, buoyancy driven
Equatorward flow	Baroclinic jets 0.4 m s^{-1} surface on shelf		Upper 200 m, 100 km wide		?	None	None	Norwegian Trench inflow
Coastally trapped waves	Period 3–10 days, speeds 2–5 m s^{-1}	5–50-day periods, MS_f period shelf wave, $c = 0.64$ m s^{-1}	No measurements		?	?	Diurnal period shelf waves west of Britain	?
Upwelling	15–34°S	8°W–2°E not related to local winds	Interacts with Canary Islands		37–43° N	Weak	Weak?	Within fjords
Filaments	Located on three main axes, interaction with rings	Freshwater plumes, $R' = 80$ km	250 km, repeatable sites, giant filament		130 km mean, 270 km maximum, 5 main sites	None	Infrequent winter dense cascades?	None
Fronts	Upwelling front, zonal Angola Front (16°S)	Three haline fronts between saline upwelling zones and ROFIs	Upwelling fronts, NACW/SACW water mass front	Water mass fronts in strait	Upwelling fronts	Plume fronts on shelf	Tidal mixing fronts and coastal current fronts on shelf, cold band at Celtic Sea break in summer	Coastal current front

TABLE I
(Continued)

	Southwest Africa (Benguela)	Equatorial West Africa	Northwest Africa	Strait of Gibraltar	Iberia	Biscay–French Shelf	NW European Shelf	Norway
Eddies	Mesoscale eddies, Agulhas rings	?	Generated in wake of Canary Islands		Generated off Cape S. Vincent	SWODDIES	Shelf-break eddies, frontal baroclinic eddies	Baroclinic eddies on coastal current front
Quasipermanent gyres	Angola Dome (cyclonic)	None	Cyclonic gyre at 17°N	Alboran gyre in Mediterranean	Over offshore banks?	None	Summer baroclinic gyres on shelf, gyres over offshore banks	?
Short-term variability	Coastally propagating atmospheric lows	Fortnightly period wave	Five upwelling events in 6 weeks		?	Tidal, springs–neaps winds events 2–5 days	Tidal, springs–neaps, 2–5-day time scale for depressions	Tidal, 2–5 days (wind)
Seasonal variability	Perennial off Namibia and south Benguela, October–March	Upwelling in June–September and December–January	20–30°N perennial winter south of 20°N		Upwelling in summer	?	Seasonal stratification on shelf, slope current stronger in winter	Freshwater discharge greatest in spring
Interannual variability	Benguela Niños (warm), 1934, 1963, 1984	Atlantic El Niño? zonal winds off Brazil	Al Mubarak		?	?	Great Salinity Anomaly	Great Salinity Anomaly
Special features	Open southern boundary, Agulhas ring interactions	Unexplained upwelling mechanism, zonal orientation or coast	Canary Islands Archipelago	Dense water outflow to 1100 m	Divided from NW Africa eastern boundary by Strait of Gibraltar	North Spain coast has zonal orientation	Extensive macrotidal shelf on an eastern boundary	Major eastern boundary buoyancy input

	South Chile, 42–55°S	Central Chile, 35–42°S	North Chile, 18–35°S	Equador–Peru, 0–18°S	North Equador–Panama, 0–9°N	Panama–Mexico	West North America	North Pacific Margin
Principal climatic influence	South Pacific High	Polar front storms, coastal lows	South Pacific High, coastal lows	ITCZ	ITCZ	ITCZ, North America Continental High	North Pacific High, Aleutian Low	Aleutian Low, North Pacific High
Principal oceanic influence	West Wind Drift (P), Cape Horn current (P)	Peru–Chile CoC (P), UC (P), SW, ESW	Peru–Chile CoC (P), UC (P)	Peru–Chile CoC, EUC	Columbia Current (P), ECC, EUC	Costa Rica CoC	California Current (E), Davidson Current (P)	North Pacific Current (P), Alaska Current (P)
Topography	100–200-km shelf, fjordic	Narrow shelf, capes, bays	Narrow shelf, capes, bays		Narrow shelf, Isthmus of Panama	Narrow shelf, three major, bays, mountain passes, Gulf of California	Narrow (10–40 km) shelf with capes, S. California Bight	Shelf 35–180 km wide, sea valleys intersect shelf, banks, Aleutian Islands
Winds	Northerly, frequent storms	Southerly, stronger in austral summer	Upwelling favorable all year	Southerly, strong diurnal signal	Equatorward in winter, offshore wind jet across Panama Isthmus	Offshore wind jets through passes	Equatorward spring and summer, poleward autumn and winter north of San Francisco	Intermittent upwelling in southern half, downwelling in north
Fresh water input	2.5 m yr^{-1} precipitation, runoff from fjords	Bio-Bio River	Arid climate	Arid zones inshore of cape–bay upwelling centers	High precipitation (ITCZ), December–April	Arid	Small, Columbia River in north	Columbia River and Juan de Fuca in south, numerous small streams, 730 $km^3\ yr^{-1}$

TABLE I
(Continued)

	South Chile, 42–55°S	Central Chile, 35–42°S	North Chile, 18–35°S	Equador–Peru, 0–18°S	North Equador–Panama, 0–9°N	Panama–Mexico	West North America	North Pacific Margin
Tides	Semidiurnal 5.5–1.5 m amplitude	Important in bays	Weak, stronger in north	Weak	Weak	Gulf of California: 9 m amplitude, solitons	Weak, stronger in north	Moderate, increasing amplitude to north
Poleward flow	Coastal current, poleward, UC detectable to 48°S	Poleward UC	Poleward UC 0.1–0.5 m s^{-1} at 100–300 m	Poleward UC over slope at 150–200 m	Columbia Current	Costa Rica CoC	California UC (shelf break), Davidson Current	Alaskan Coastal Current, Alaska Current (slope), Vancouver Island CoC
Equatorward flow	None	Upper 20 m on shelf during upwelling	Humbolt Current (little influence on CoC)	Confined to upper 25–50 m on the shelf	Annual El Niño Current		Seasonal California Current, upwelling jets	Coastal current reversals
Coastally trapped waves	?	?	<0.2 cycle day^{-1}, $c = 2.8–3.8$ m s^{-1}	$c = 2–3$ m s^{-1}, clearest in winer during non–El Niño conditions	Equatorial origin, currents not with local winds	Present	Wind driven 3–10-day period, source 200–300 km equatorward.	Present, diurnal shelf wave off Vancouver Island
Upwelling	Downwelling, possible upwelling within fjords	35–38°S, especially in equatorward-facing bays	In bays and points at SW ends of bays, within 60 km of coast	Major centers 6°S, 9°S, 12°S, 15°S	Generally downwelling, upwelling north of 4°N in boreal winter	Heads of gulfs of Papagayo, Tehuantepec	Upwelling 35–50°N, spring and summer, winter and spring in southern California	Downwelling

Filaments	None	50–150 km offshore	Extending 40–60 km upwelling centers, occasionally 75–125 km	Extend 25–50 km from upwelling centers, retreat after wind relax	Caused by offshore wind jets	Caused by offshore wind jets	50–300 km (20–40 days) often at promontories related to instabilities	Squirts from coastal current instabilities
Fronts	?	Upwelling and plume fronts		No upwelling fronts or jets, equatorial front (strongest in austral winter)	Equatorial front	In Gulf of California	Upwelling and buoyancy fronts, meander jets	Coastal current front
Eddies	?	Punta Lavapié	?	?	?	Spun up from offshore filaments dipole anticyclonic dominant	Generated by instability	Dipole eddies on coastal current front, Juan de Fuca eddy
Quasipermanent gyres	None	?	?	?	Panama Bight gyre (cyclonic)	Costa Rica Dome (cyclonic)	Southern California eddy (cyclonic)	Sitka eddy, Kayak eddy (anticyclonic)
Short-term variability	Storm events	Upwelling events 2–7 days	3–10-day poleward propagating atmospheric lows	8–11 days (CTW), 3–10 days wind fluctuations		Offshore wind jets 3–4 days	3–10-day wind driven on shelf, 20–60 days over slope	Storms

TABLE I
(*Continued*)

	South Chile, 42–55°S	Central Chile, 35–42°S	North Chile, 18–35°S	Equador–Peru, 0–18°S	North Equador–Panama, 0–9°N	Panama–Mexico	West North America	North Pacific Margin
Seasonal variability	More seasonal in north with precipitation greater in winter	Upwelling in summer	Upwelling strongest in spring	Peru CoC strongest in spring, upwelling strongest in winter	Winter ITCZ at 7°N, summer ITCZ at 1°N	Offshore wind jets in winter	Wind direction: abrupt spring transition	Freshwater runoff: maximum autumn, minimum spring
Interannual variability	?	El Niño effects extend to 37°S	El Niño	El Niño, stronger poleward flow, faster CTWs	El Niño	El Niño	El Niño	ENSO, 6–7-year atmosphere cycle, 18-year lunar cycle
Special features	Open southern boundary	Low O_2 in upwelled water	Low O_2 in upwelled water	Low O_2 in Upwelled water		Strongly influenced by offshore wind jets	Straight, simple coast (northern 1500 km), little freshwater input	Major buoyancy input on eastern boundary

[a] CC, countercurrent; CoC, coastal current; CTW, coastally trapped wave; E, equatorward flowing; ECC, Equatorial Countercurrent; ENSO, El Niño–Southern Oscillation; ESW, Equatorial Surface Water; EUC, Equatorial Undercurrent; ITCZ, Inter-Tropical Convergence Zone; MS_f, lunisolar fortnightly tidal constituent; NACW, North Atlantic Central Water; NECC, North Equatorial Countercurrent; P, poleward flowing; ROFI, region of freshwater influence; SACW, South Atlantic Central Water; SWODDIES, shelf-water ocean eddies; UC, undercurrent.

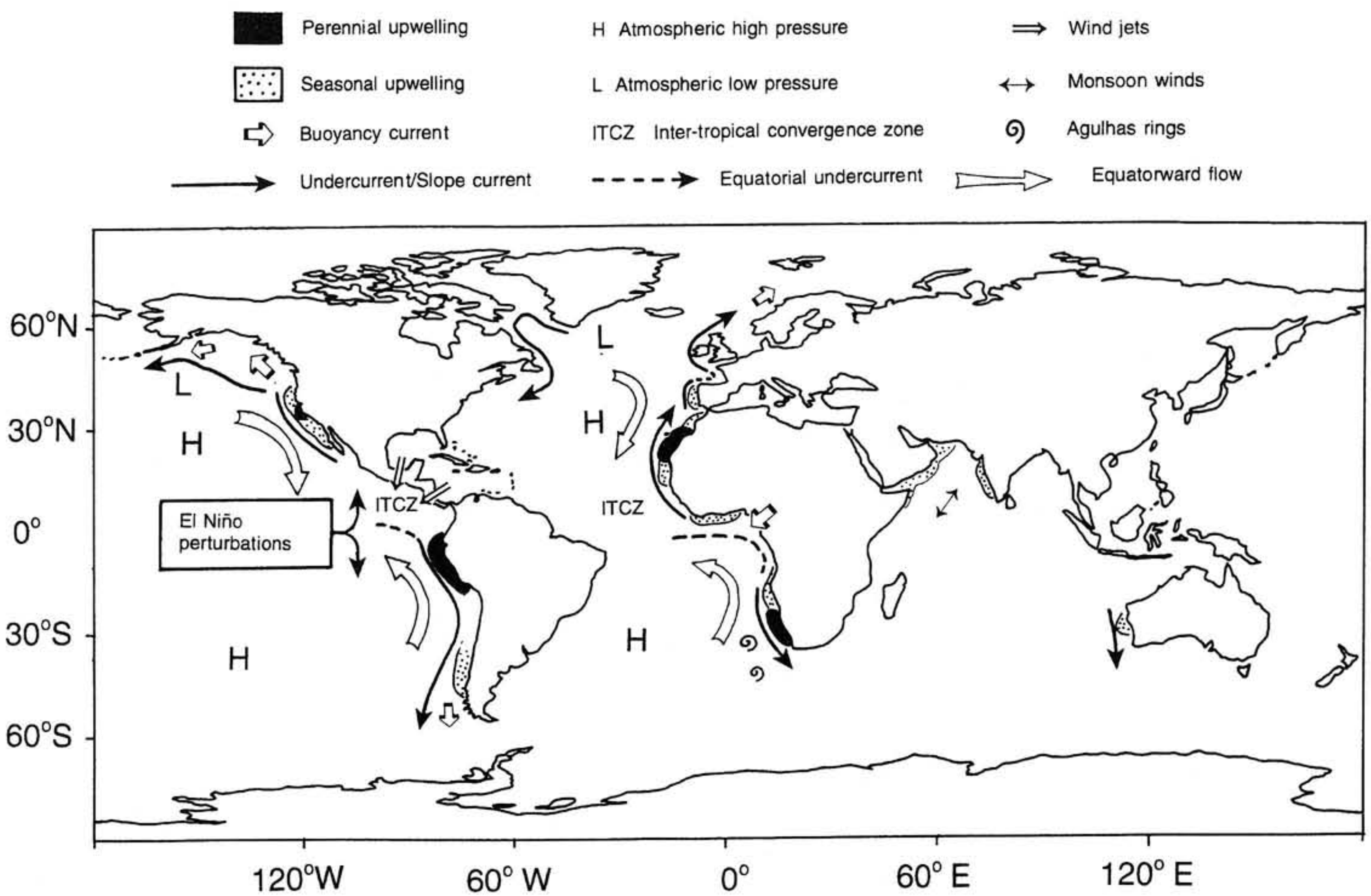

Fig. 2.1. Global map showing the ocean eastern boundaries and phenomena. In this figure the poleward undercurrents and slope currents are drawn some distance offshore for clarity. However, these currents are invariably located over the continental slope or on the shelf, and so are usually quite close to the coast.

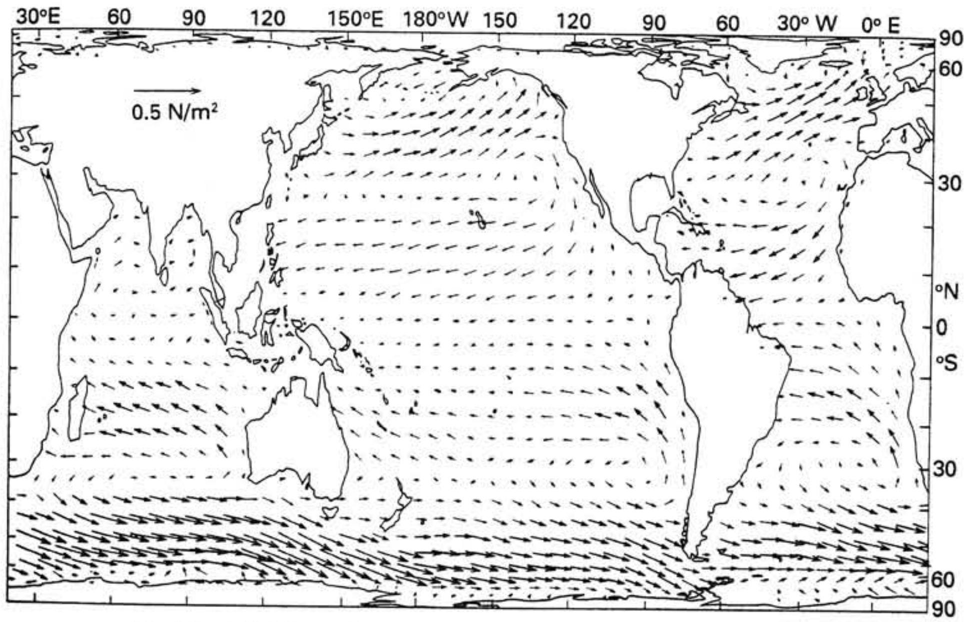

Fig. 2.2. Global annual mean winds. (From Tomczak and Godfrey, 1994.)

in each hemisphere, however, meridional shifts in the atmospheric highs mean that the equatorward wind forcing reverses seasonally to become poleward in autumn and winter (e.g., Iberia, Pacific northwest from 38 to 50°N and southern Benguela). At higher, subpolar latitudes, where weather systems are controlled by atmospheric low-pressure systems, winds are generally downwelling favorable on eastern boundaries. Cyclonic atmospheric depressions that grow on the polar fronts produce frequent storm events with high precipitation, particularly in winter (e.g., northwest Europe, southern Chile, Alaska, and southern South Africa). In equatorial regions the Inter-Tropical Convergence Zone (ITCZ) is responsible for weak, variable winds and high precipitation. Important seasonal changes occur, however, as a result of the seasonal north–south movement of the ITCZ toward the summer hemisphere. In the Indian Ocean, the annual monsoon cycle is responsible for major seasonal modulation of both wind and buoyancy forcing.

On longer time scales, intermittent, interannual changes in large-scale atmospheric pressure gradients over the Pacific Ocean result in relaxation of the easterly wind stress over the western equatorial Pacific. This and the associated events are termed ENSO (El Niño–Southern Oscillation). For a general description of the El Niño phenomenon in the Pacific, the reader is referred to the review by Strub et al. (Chapter 10). In the ocean, El Niño events are manifest by the eastward propagation of equatorially trapped Kelvin waves, which have dramatic effects when they impinge on the eastern Pacific boundary: coastal sea levels rise by up to 0.5 m, the thermocline (and nutricline) is depressed by 50–100 m, surface waters warm by about 5°C and coastally trapped Kelvin waves propagate the El Niño disturbance considerable distances (on the order of thousands of kilometers) poleward on both sides of the equator. Depression of the nutricline means that in regions affected by El Niño, upwelling draws on nutrient-poor waters from above the nutricline so that primary and secondary production drops, with consequent impacts on the rest of the marine food chain. In El Niño years nutrient levels in some eastern boundary regions (e.g., California Current) may also be affected by large-scale changes in lateral advection in the equatorward eastern boundary current system. A similar but less frequent phenomenon occurs in the South Atlantic (Benguela Niños), leading to poleward intrusions of warm surface Angolan water which, near the bottom, appears to be low in oxygen. At higher latitudes (e.g., northwest Pacific margin) it is probable that the observed coastal changes in El Niño years are brought about not only by direct transmission of the oceanic El Niño signals by freely propagating Kelvin waves, but also by atmospheric teleconnections (changes in the basin-scale wind field brought about, for example, by expansion and intensification of the Aleutian Low and diminution of the Pacific High). These large-scale changes influence the coastal ocean by altering the local atmospheric forcing (wind and heat flux; e.g., Chapter 12).

Just as the deep ocean exhibits east–west asymmetry in both steady and time-dependent flow components due to the planetary beta effect (western intensification and westward planetary wave propagation), a similar dynamical asymmetry is found along eastern boundaries due to the topographic beta. The phase propagation of coastally trapped waves is poleward, and in the steady state, poleward-flowing, slope-trapped currents are ubiquitous on eastern boundaries.

3. Eastern Boundary: Processes and Phenomena

Table I summarizes the principal oceanographic phenomena observed on eastern boundaries and illustrates the high degree of commonality between regions. Certain phenomena, such as coastal-upwelling, poleward-flowing undercurrents and coastally trapped waves, are prevalent in many regions (Huyer, 1990; Brink, 1997). In the following sections the main phenomena and the processes that regulate them are examined briefly, although many of these are closely interrelated.

3.1. Upwelling

The basic mechanism of wind-driven coastal upwelling is well understood. Equatorward winds induce net offshore surface Ekman transport, which brings about transport divergence near the coast. The Ekman transport is usually quantified in terms of the *upwelling index*, which is a long-term average at a given location of monthly mean Ekman transports derived from observed winds and expressed in units of $m^3\ s^{-1}$ per 100 m of coastline. In upwelling systems this index is typically on the order of 100 (offshore). Figure 2.3*a* illustrates the classical two-dimensional, two-layer upwelling model with a deep lower layer. The pycnocline depth is h_0 far from the shore, and the ocean is forced by a steady, uniform, equatorward wind stress, τ_{sy}. A fuller account of upwelling dynamics is given by Brink (1997). The key features are (1) offshore surface layer transport far from the coast, (2) zero cross-shore transport at the coast, (3) an uplifted pycnocline close to the coast, and (4) a geostrophic equatorward coastal current. Moreover, the model quantifies what is meant by "close to the coast"; the width scale of the pycnocline uplift (and the associated coastal jet) is the baroclinic Rossby radius of deformation, $R' = (g'h_0)^{1/2}/f$, characteristically 5–20 km. The vertical upwelling velocity (rate of pycnocline uplift) is readily deduced from continuity as $w = O(\tau_{sy}/\rho f R')$. Since the wind stress in upwelling systems is characteristically

0.1 N m^{-2}, a characteristic midlatitude upwelling velocity is 10 m day^{-1}. When the pycnocline eventually breaks the surface it tends to move offshore, leaving a band of (cold) upwelled water against the coast separated from warm offshore waters by an upwelling front of width R' (Fig. 2.3*b*). It appears (DeSzoeke and Richman, 1984) that the main factor governing the width of the cold upwelling band is the time-integrated offshore Ekman transport, so that the band tends to be narrower off Oregon, where the upwelling-favorable winds are intermittent, and weaker than off California, where the winds are steadier and stronger (Chapter 12). However, other factors, such as the larger-scale circulation, undoubtedly play a role. The Chilean upwelling system is exceptionally narrow compared with other midlatitude systems, possibly under the influence of the offshore circulation regime (Chapter 10). An extreme case is the Leeuwin Current region off western Australia, where upwelling-favorable winds exist but upwelling is not observed (e.g., Godfrey and Ridgway, 1985), We still have much to learn about the processes governing the net offshore transports associated with upwelling. The upwelling front is in approximate geostrophic balance, which implies an equatorward, frontal baroclinic jet with speeds on the order of 0.1–0.5 m s^{-1} (Fig. 2.3*b*). The exception to this pattern is the upwelling system off Peru, which lacks a strong upwelling front for possible reasons discussed by Strub et al. (Chapter 10). Off southern California the upwelling front is generally so far offshore that the usual measurements made over the shelf rarely detect it. However, there is coastal upwelling within the Southern California Bight, usually in winter and early spring, and during these events there is an upwelling front close to the coast. Unusually, the upwelling occurs in winter because in the Southern California Bight, the winds are reduced in summer by orographic effects.

The simplified (reduced gravity) model accounts for many of the essential features of upwelling systems. Not only is upwelling well understood qualitatively, but the offshore flow at the surface agrees quantitatively with Ekman theory as long as the observed offshore flow includes not only the surface mixed layer but also flow in the transition region beneath the mixed layer (Lentz, 1992). Several important aspects of upwelling are not, however, reproduced by the simple upwelling model. For example, coastal upwelling usually occurs over a shallow continental shelf where bottom topography and frictional effects are important (Fig. 2.3*c*,*d*). In particular, over a shallow shelf with a finite lower-layer depth, an on–off shelf component of flow in the lower layer can be expected (unlike in the deep, lower-layer case, where pycnocline adjustment can occur while the horizontal lower-layer velocities remain negligible; Fig. 2.3). The onshore lower-layer motion supplies the transport of upwelling water, which typically comes from 50–250 m depth. If in shallow water, the equatorward coastal current penetrates the entire water column, the bottom Ekman layer transport it induces is onshore and hence can supply the upwelling water (Fig. 2.3*c*). On the other hand, strong poleward flow is usually present in upwelling systems (see the next section), and if this penetrates the shelf (e.g., Benguela, California Current, central Chile), the bottom Ekman layer transport is offshore. In the latter circumstances, there is offshore transport in both surface and bottom Ekman layers (Fig. 2.3*d*) and the onshore supply of upwelling water is necessarily at middepth, such as off Peru (Chapter 10). Bottom boundary layers are somewhat more complex and less understood in upwelling regions, producing vertical density structures that are not symmetric during upwelling versus downwelling conditions (Lentz and Trowbridge, 1994). Similarly, the inner shelf region, where surface and bottom boundary

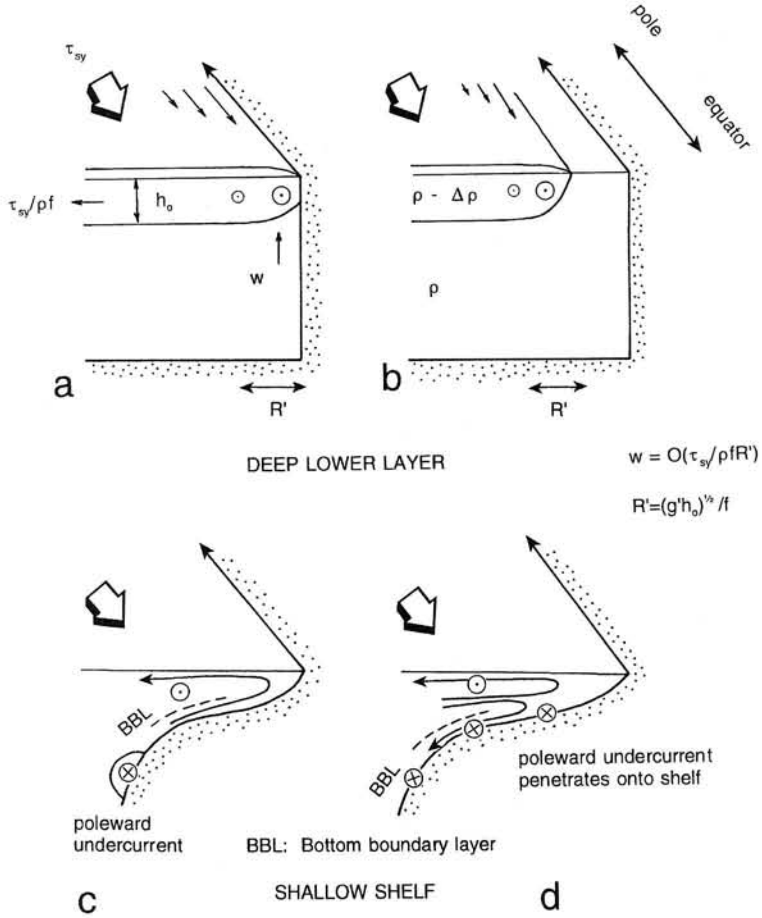

Fig. 2.3. Schematic of coastal upwelling: (*a*) two-layer upwelling model with a deep static lower layer showing pycnocline uplift at the coast; (*b*) two-layer case showing the upwelling front displaced offshore; (*c*) upwelling over a shallow frictional shelf; the equatorward flow on the shelf penetrates to the bottom and bottom Ekman layer transport is onshore, supplying the upwelling waters; (*d*) upwelling over a shallow frictional shelf when the poleward undercurrent penetrates the shelf; bottom Ekman layer transport is offshore and upwelling waters are supplied from middepth.

layers overlap, has received less attention, but the cross-shelf flow appears from one study at least to be more two-dimensional than the flow at midshelf (Lentz, 1994). More studies are needed of both the bottom boundary layers and the inner shelf (see Trowbridge et al., 1997).

The steady-state model provides only partial insight into coastal upwelling regimes, which are highly time-dependent systems that respond rapidly to wind stress fluctuations. Upwelling actually takes place as a series of (typically, 3 to 10-day) events, during which vertical velocities are maximum (order 10 m day^{-1}). A particularly dramatic example of time dependence is the *spring transition* in the northern part of the California Current system, in which the large-scale (1500 km) wind field switches from poleward to equatorward over just a few days causing an abrupt sea-level drop, reversal of the surface current direction from poleward to equatorward and uplift in isopycnals toward the coast (Chapter 12; Huyer et al., 1979). Another source of time dependence in upwelling systems is brought about by the propagation of disturbances from remote locations by coastally trapped waves (see later) which induce variability on time scales of from 3 to 10 days. The seasonality of upwelling events is controlled by meridional shifts in subtropical atmospheric highs. In the central subtropical region, upwelling is year-round (perennial), but even so, exhibits a seasonal variation. At the poleward and equatorward margins of this zone, upwelling is strongly seasonal. In this context, *seasonal* refers to the fact that upwelling appears only in some seasons, or even where it occurs all year, is usually stronger in one season.

Figure 2.4 provides a schematic of some of the important processes occurring in upwelling systems and is similar to the classic picture of Hart and Currie (1960). Based on more recent insights, however, the figure emphasizes the fundamentally three-dimensional nature of these systems, which have marked alongshore variability

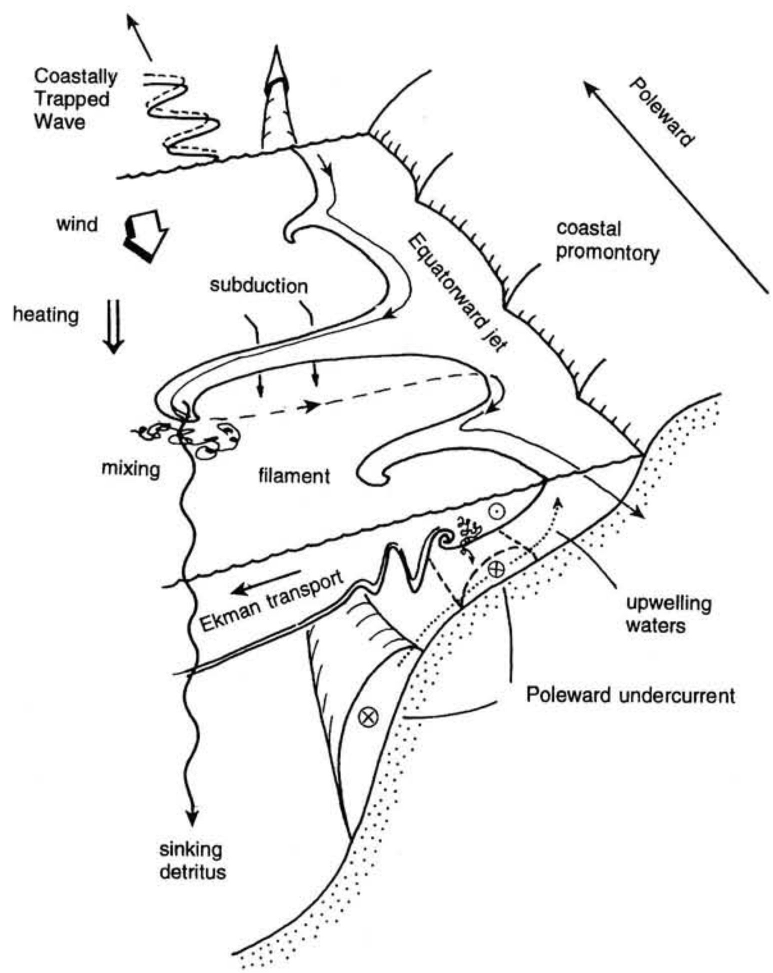

Fig. 2.4. Schematic of an upwelling system.

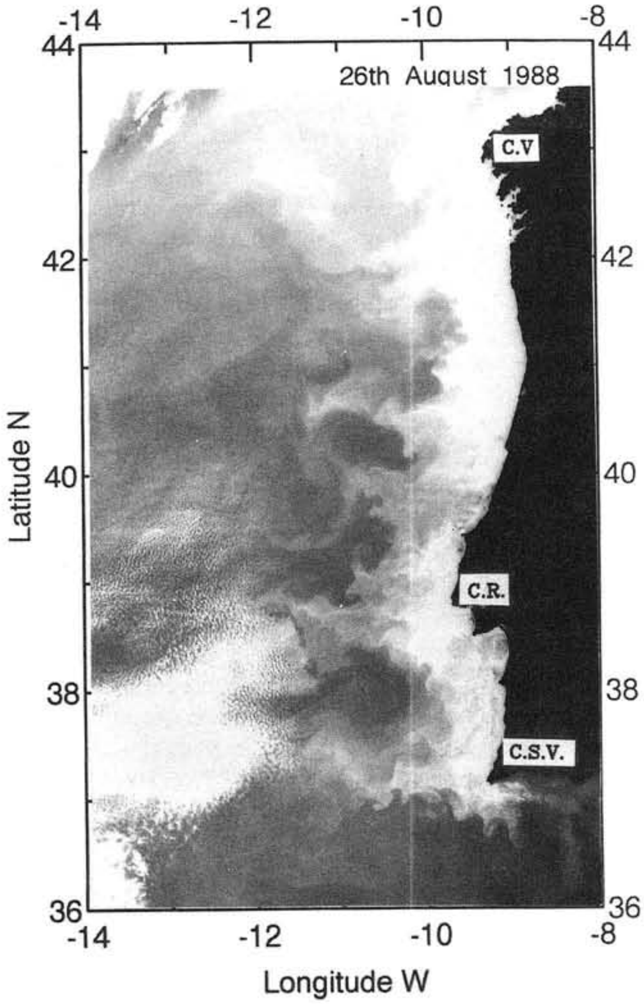

Fig. 2.5. Satellite infrared image from August 26, 1988, showing cold (light tone) upwelled waters against the Iberian coast with upwelling filaments extending offshore. C.V., Cape Finisterre; C.R., Cabo Roca; C.S.V., Cabo São Vicente.

with onshore–offshore flows rarely in mass balance on a given section. A particular source of alongshore variability is the instability of the equatorward baroclinic jet (along the upwelling front). In the mid-1970s large-scale filaments of cold coastal water were observed in satellite infrared images extending 50–300 km offshore in the California upwelling system and with an alongshore separation scale of about 200 km. Figure 2.5 shows an infrared satellite which reveals upwelling filaments off Iberia (e.g., Haynes et al., 1993), and a further such image from the California Current can be seen in the review by Hickey (Chapter 12). The existence of these structures, their penetration to depths of 200 m or more, and the strong offshore velocities (squirts) within them have been confirmed by ship surveys (Chapter 12; Flament et al., 1985; Brink and Cowles, 1991, and other papers in the same volume). Transport estimates across filaments in the California Current are in the range 1.5–3.6 × 10^6 m^3 s^{-1} (Kosro and Huyer, 1986). Table I demonstrates that filaments are found in all other major eastern boundary upwelling systems. The time scales of such structures are typically in the range 10–60 days. Filaments can be produced by many processes and several competing hypotheses have been advanced to explain their dynamical origin. These include topographically induced meanders of the mean flow, motion induced by offshore eddies and instability of the frontal jet (possibly initiated by coastal features such as promontories). Agulhas rings shed from the Agulhas Current retroflection south of Africa travel into the South Atlantic Ocean and can interact with the Benguela frontal region to form extremely long filaments (Chapters 19 and 20). The filaments off Peru are smaller and have shorter time scales than many other upwelling filaments and are not geostrophic but are surface plumes driven directly by the wind. The California Current and Iberian filaments are probably brought about by frontal jet instability. Although superficially the squirts appear to transport cold, upwelled water offshore into the open ocean, it may be that at least some of the filaments observed are merely part of a large-scale meander in which the offshore-moving water is eventually returned on-shelf. Only the off-shelf segment of the meander appears in satellite infrared images because the warming and sinking of cold filament surface waters during the offshore leg means that there is little surface temperature contrast during the onshore motion (Brink and Cowles, 1991). Despite this, some irreversible mixing of filament and ocean waters will occur, so that filaments can be expected to play a role in the exchange of water properties between the shelf and ocean (Huthnance, 1995). Moreover, during the time (weeks) that nutrient-rich filament water spends over the deep ocean, high levels of primary production can be expected, and this will contribute to the direct flux of carbon to deep-ocean sediments even though the water itself may eventually return inshore.

3.2. *Poleward Flow*

Table I illustrates the ubiquitous nature of poleward flow on eastern boundaries (Neshyba et al., 1989). Some of these flows are due to region-specific local forcing, such as buoyancy-driven coastal currents. However, the extensive nature of eastern boundary poleward currents, which often flow against prevailing equatorward winds, suggests that a larger-scale, nonlocal forcing mechanism may be at work. Figure 2.4 shows how a poleward undercurrent beneath the generally equatorward wind-driven surface layer is characteristic of coastal upwelling systems. Usually, the poleward undercurrent is located at the shelf break or over the continental slope with a width on the order of 20–100 km and current speeds of order 0.1 m s^{-1}. Sometimes the poleward flow penetrates the shelf to occupy the lower layers (e.g., Benguela, northwest Pacific). Off northwest Africa there are indications that the undercurrent becomes weaker and its core deeper in the poleward direction, whereas in other locations, such as the slope current off northwest Europe, the flow becomes stronger and its core shallower in the poleward direction. The wider significance of the poleward undercurrent for upwelling systems is that it is often the source from which upwelled waters are drawn. Off central Chile, for example, low-oxygen waters in the poleward undercurrent, when upwelled against the coast, have caused fish kills (Chapter 10). In the California Current system the poleward undercurrent is thought to play a role in the instability of the alongshore jet by providing a strong source of baroclinic instability (vertical shear). Pingree and Le Cann (1992) have shown that anticyclonic eddies of shelf–slope water (SWODDIES) with characteristic radii of 50–60 km are shed from the (surface) continental slope current off northern Spain and propagate into the ocean, where their signature is discernible in the upper 1500 m and where they persist with a lifetime of about one year.

Given the association of poleward flows with upwelling systems, one class of models seeks to explain the undercurrent as an integral part of the eastern boundary upwelling response (e.g., McCreary, 1981). The simple upwelling model (Fig. 2.3) is a useful reference point since it shows no undercurrent. Indeed, no two-dimensional upwelling model (i.e., one without alongshore variability) is capable of reproducing a poleward current simply as part of the response to equatorward winds. However, poleward lower-layer flow could be brought about by application of either an alongshore surface slope (sea level declining poleward) or an offshore pressure gradient (sea level rising toward the coast). As we shall see later, alongshore oceanic surface slopes induce cross-shore slopes from shelf to ocean, so the two forms of pressure gradient are not independent (see also Hill, 1997). Along-slope variations in topography could, for instance, allow the necessary alongshore pressure gradient to drive the poleward undercurrent. Similarly, alongshore variations in wind stress could establish alongshore pressure gradients (e.g., McCreary, 1981). Since there is always some along-slope variability in both topography and forcing, a partial explanation for the poleward undercurrent may lie with the foregoing mechanisms. However, there are notable regions where upwelling and equatorward flows are absent but the poleward current is still present (e.g., Oregon, Iberia in winter and the northwest European shelf edge year round). Moreover, in a great many cases (even on western boundaries) the undercurrent or slope-trapped current, regardless of the prevailing wind direction, flows in the same sense as that of coastally trapped wave propagation (shallow water to the right/left in the Northern/Southern Hemisphere). This suggests that in many cases we have to look beyond wind forcing for an explanation of these phenomena.

A clue to the possible origin of the poleward flow is provided by the Leeuwin Current. Warm equatorial waters pile up at the northern margin of western Australia, due to the Indian–Pacific surface flowthrough component of the global thermohaline circulation. The resulting alongshore oceanic pressure gradient drives oceanic water toward Australia and so forms the Leeuwin current, which flows southward (poleward) down the Western Australian coast (McCreary et al., 1986). As the current flows southward it cools and the steric height drops, maintaining the meridional pressure gradient (Tomczak and Godfrey, 1994). In this area the near-bottom current is equatorward rather than poleward as in the other eastern boundary upwelling systems. This example suggests an alternative model in which large-scale meridional pressure gradients, established in the open ocean, rather than complex responses to wind forcing, drive poleward flows.

Steady-state adjustments between oceanic pressure gradients and the coastal zone can be interpreted in terms of Csanady's (1978) arrested topographic wave model. Using this approach, Wang (1982) neatly demonstrated that an alongshore pressure gradient imposed in the deep ocean, adjacent to a steep continental slope, would fail to penetrate the shelf. The argument is based on an analogy between the equation governing the steady sea-level field (the arrested topographic wave) and the heat conduction equation. For uniform slope, the extent of the penetration of alongshore oceanic sea-level gradients onto the shelf is governed by an analog of the thermal conductivity, $K = r/fs$, where r is a friction coefficient and s is the bottom slope. Steep slopes (large s) thus inhibit transmission of the oceanic sea-level field to the shelf. In these circumstances, shelf–ocean sea-level adjustment is confined to the slope region and results in a slope-trapped current. The arrested topographic wave analogy with heat conduction problems also means that slope currents can spread only in the direction of topographic wave propagation (poleward on eastern boundaries). Moreover, the effects of "upstream" sea-level disturbances are felt downstream over distances of order 1000 km or more. These effects seem to be mitigated if density stratification is present, in that surface-intensified flow patterns begin to be attenuated only once the flow contacts the bottom (Kelly and Chapman, 1988).

Huthnance (1984, 1995) has examined the problem starting with the assumption that the oceanic sea-level gradient is physically due to the meridional drop in steric height arising from the fall in ocean temperatures poleward. In these circumstances, when zonally oriented density surfaces intersects a meridional sloping boundary, the dynamical adjustment of the density-induced pressure gradient to the bottom slope is termed the *joint effect of baroclinicity and relief* (JEBAR) or *pycnobathic forcing* (Hill, 1997). Assuming no net cross-shore transport, and supposing that the same meridional density gradient affects both ocean and shelf, the alongshore sea-level slope is proportional to the bottom depth (for further explanation, see Hill, 1997). Sea level thus declines more slowly on the shelf than in the deep ocean, so that an offshore pressure gradient develops between the shelf and the ocean which drives poleward flow along-slope. The sea-level difference between shelf and ocean increases along-slope (until frictional influences eventually come into play), hence the poleward current is expected to strengthen along-slope. The JEBAR mechanism should apply along the entire eastern boundary but would seem most relevant just upstream of regions where steric height drops markedly due to cooling at the poleward margins of the eastern boundaries (e.g., off northwest Europe, where there is intense cooling in the Norwegian Sea farther north). One consequence of a model in which slope currents are driven by the large-scale oceanic meridional pressure gradient is that where the slope orientation is zonal (e.g., northern Spain), the along-slope component of the pressure gradient is eliminated and slope current strength ought to weaken (Pingree and Le Cann, 1989). The role of JEBAR, if any, in the generation of slope currents remains uncertain at present.

A third class of model interprets poleward-flowing eastern boundary currents in terms of rectification of time-dependent motions over the sloping boundary. Rectification of the cross-slope component of the oscillatory barotropic and internal tides can induce along-slope Eulerian flow, again in the direction of topographic wave propagation (e.g., Loder, 1980). Moreover, ever-present subinertial time-dependent flows over irregular bottom topography rectified by *form stress* along a sloping continental margin can also produce alongshore flow in the direction of topographic wave propagation under quite general conditions (Haidvogel and Brink, 1986; Holloway, 1987; Holloway et al., 1989).

Observations of the poleward current on eastern boundaries are limited to several well-studied locations, and the question remains as to whether the observed segments of poleward flow are actually part of a continuous eastern boundary current system. In some locations water mass analysis provides a clear answer. For example, the low-oxygen poleward undercurrent off South America appears to be a continuous feature, as does the California Undercurrent, which can be traced hundreds of kilometers by its warm, saline, oxygen- and nutrient-poor signature. However, in other cases (e.g., Iberia) there are considerable water mass variations on sections with small along-slope separations. It may be that the eastern boundary circulation consists of a number of distinct (horizontal) cells, each with poleward flow at the eastern boundary margin but with limited flow continuity between them (Huthnance, 1995). Even if the poleward current is continuous in the Eulerian sense, this does not imply continuity in the Lagrangian sense since an individual water parcel can be mixed offshore or recirculated in a variety of ways. The issue of poleward flow continuity on the North Atlantic eastern margin has a particular focus because the African and European boundaries are physically separated by the Strait of Gibraltar and the Gulf of Cadiz. Is there continuity between the northwest African and Iberian poleward flows? Moreover, how would the undercurrent interact with the cascade of dense Mediterranean Intermediate Water, which itself descends the continental slope and flows poleward as a core at about 1100 m?

The term *poleward undercurrent* has been used repeatedly in this section because most eastern boundary poleward flows are subsurface features with a core, typically at around 300 m, capped in upwelling regions by equatorward-flowing surface waters. There are regions, however, where the poleward current breaks the surface. The Davidson Current (Hickey, 1979), for example, flows poleward over the shelf and slope at the surface in winter, counter to offshore equatorward surface flow. Off northwest Europe there is no equatorward surface flow, and the term *slope current* is widely used to emphasize the slope-trapped nature of the flow at the shelf edge. The nomenclature of eastern boundary currents tends to obscure the high degree of commonality between all these forms of poleward flow, which are probably different manifestations of essentially the same phenomenon. Indeed, the common link between eastern boundary poleward flows probably extends beyond the eastern boundary itself. The western boundary currents associated with the subpolar gyres (such as the Labrador Current and the Falkland–Malvinas Current) have similarities with eastern boundary slope currents. The common link is that they all flow in the direction of topographic wave propagation, which is equatorward on a western boundary (clearly, the Gulf Stream is not a member of this family of currents). These western boundary currents tend to be slope trapped and can usefully be modeled using arrested topographic wave dynamics in the sense that prescribed upstream inflows evolve downstream into realistic slope-trapped flow fields in relation to the topography (e.g., Greenberg and Petrie, 1988). The Labrador Current is a particularly pertinent case because it is probable that this western boundary flow is the downstream extension of a larger subpolar, slope-trapped current system that is ultimately continuous with the West Greenland Current, an eastern boundary current (Chapman and Beardsley, 1989).

There are several examples of temporal variability in the poleward undercurrent. On short time scales, for example, coherent 7 to 20-day fluctuations in both the Equatorial Undercurrent and the poleward undercurrent off South American provide evidence of a connection between these two systems and highlight the importance of the Equatorial Undercurrent as an oceanic influence off South America (Huyer et al., 1991). A clear example of seasonal variability in poleward flows is provided by the Davidson Current (California), which flows between 35 and 50°N in autumn and winter, replacing the equatorward surface flow that occurs in spring and summer. It has been suggested that the Davidson Current is a result of surfacing of the California Undercurrent in late autumn (Chapter 12). The California Undercurrent (the slope poleward flow) has a clear seasonality with maximum poleward flow in summer to early autumn and minimum in spring (Chapter 12). A situation similar to the Davidson Current arises off Iberia, where temporary relaxation of the summertime trades allows the development of a northward (poleward)-flowing current along the outer shelf and slope; this current dominates during winter. The slope current off northwest Europe has its maximum velocities, is closest to the surface and has its maximum encroachment onto the shelf during winter.

3.3. *Buoyancy-Driven Coastal Currents*

An account of buoyancy-driven coastal currents and their dynamics is given by Hill (1997). The principal freshwater buoyancy-driven coastal currents are on the fjordic high-latitude eastern boundaries (e.g., the Norwegian Coastal Current, the Alaskan Coastal Current, the Vancouver Island Coastal Current, the Columbia river plume in winter and the Fjord Current system of southern Chile). Summer flooding of the Orange River (South Africa) can also produce intermittent buoyancy-driven coastal flows. The major freshwater buoyancy input of the Niger and Zaire Rivers produces extensive plumes, reducing the surface salinity in the Gulf of Guinea. Proximity to the equator, however, means that the influence of the earth's rotation is relatively small (the baroclinic Rossby radius is 80 km), and these plumes tend not to form well-organized coastal currents. The freshwater plumes do, however, interact with coastal upwelling centers and pronounced offshore-oriented fronts separate the plumes from salty upwelled waters (Chapter 21).

Buoyancy-driven coastal currents generally have a wedge-shaped density structure with the sea surface sloping downward offshore (Fig. 2.6). Provided that the coastal current is sufficiently large, the alongshore flow is in approximate geostrophic balance, so that on eastern boundaries, buoyancy currents also flow poleward. The width scale of buoyancy-driven coastal currents is also expected to be on the order of the baroclinic Rossby radius, although major buoyancy-driven coastal currents (e.g., Alaska, Norway) are observed to be much wider than this (Hill, 1997). Upwelling-favorable winds (see later) can also dramatically spread buoyant plumes offshore (Münchow and Garvine, 1993; Hill, 1997; Hickey et al., in press). The frontal boundaries of buoyancy currents are usually baroclinically unstable and spawn Rossby radius–scale eddies. These have the form of cyclone–anticyclone pairs (Griffiths and Linden, 1982) and play a role in entraining ocean water into coastal currents, causing them to widen beyond the Rossby radius scale. Norwegian Coastal Current eddies have swirl velocities up to 1 m s^{-1} which are regarded as hazardous in towing operations involving offshore oil and gas platforms. High-latitude eastern boundary buoyancy currents are thus an important source of mesoscale eddy activity.

Buoyancy-driven coastal current systems are affected by other forcing mechanisms. For example, the Norwegian Coastal Current is influenced by wind events both directly and through the influence of the wind on the buoyancy supply. Transports of these currents thus vary with the seasonal cycles of freshwater discharge and wind stress, although shorter time-scale fluctuations in buoyancy sources can also be a source of variability (Hickey et al., 1991). In the Alaskan Coastal Current system, buoyancy and wind forcing are out of phase with maximum freshwater input in autumn, followed by maximum (downwelling-favorable) wind stress three months later. Cross-front density gradients are thus enhanced by freshwater discharge and then further enhanced by the winds, leading to an increase in alongshore baroclinic

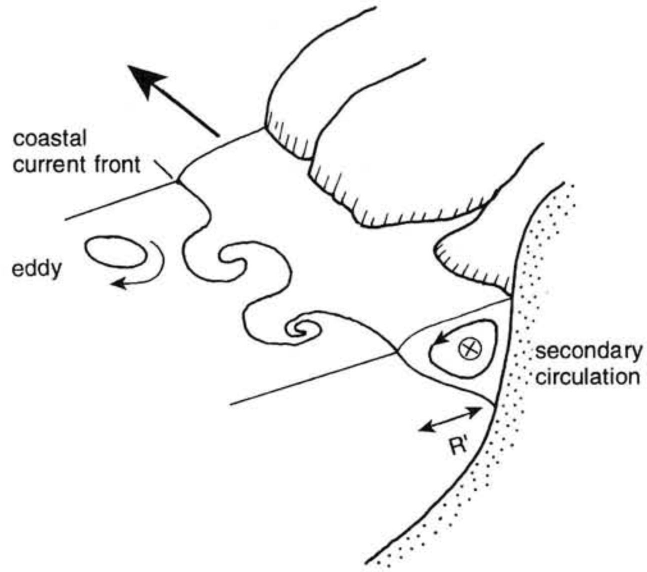

Fig. 2.6. Schematic of a buoyancy-driven coastal current.

flow. Westerly winds can block Baltic Sea outflow, which when winds eventually relax, flows out around the Norwegian coast in a borelike pulse. The primary source of current variability is the wind, however, which causes fluctuations on time scales of several days and can cause complete reversal of the Alaskan Coastal Current on occasions (Chapter 13). The response of the Columbia River (Pacific west coast) to variable forcing has recently been investigated (Chapter 12). The Columbia River plume reverses seasonally, flowing generally southward well offshore of the shelf during summer (against the direction expected for a buoyancy-driven flow) and generally northward in winter. The portion of the plume over the shelf responds rapidly to changes in wind and/or ambient currents, tending northwest of the river mouth and thinning to 5–10 m under conditions of upwelling-favorable winds during winter, but tending northward against the coast and thickening to 20–30 m during winter storms (Hickey et al., in press). When the strength of the seasonal equatorward coastal jet increases in spring, the plume tends due west of the river mouth and then bends equatorward in the California Current offshore of the shelf. In contrast, the Vancouver Island Coastal Current flows northward in summer (as expected for buoyancy flows) against the direction of the prevailing equatorward winds (Chapter 12; Hickey et al., 1991).

The large-scale eastern boundary undercurrents and slope currents transport warm waters poleward, and consequently, large-scale lateral density gradients are maintained across them (i.e., arising not merely from localized buoyancy input). The Northwest European Slope Current, for example, has the form of a wedge of warm (buoyant) water with a saline core against the upper slope (Hill and Mitchelson-Jacob, 1993). Similarly, the California Undercurrent transports warm, salty, oxygen- and nutrient-poor waters poleward along the Pacific west coast (Chapter 12; Hickey 1979). In this wider sense, therefore, buoyancy forcing is an aspect of many eastern boundary poleward flows.

3.4. *Coastally Trapped Waves*

A key finding in a number of eastern boundary regions (e.g., Peru, California) is that variability in coastal sea-level and alongshore currents is not simply a direct response to local wind forcing (on a days to weeks time scale). The picture is sometimes confused because where the winds have large spatial scale (e.g., California), correlations with local winds can appear high, obscuring the distinction between local and remote forcing. For example, in the California Current system the variance in the most energetic band on the shelf (3–10 days) is wind forced, but the forcing occurs several hundreds of kilometers farther south (Denbo and Allen, 1987). Such fluctuations in currents and sea levels are usually interpreted in terms of free-propagating, long-period waves (Allen, 1980; Battisti and Hickey, 1984; Brink, 1991, 1997). The alongshore (depth-averaged, linearized) momentum balance in the coastal ocean is given by

$$\frac{\partial v}{\partial t} = -\frac{1}{\rho_0}\frac{\partial p}{\partial y} - fu + \frac{\tau_{sy}}{\rho h} - \frac{\tau_{by}}{\rho h} \tag{1}$$

where y is the alongshore direction (u, v) are cross- and alongshore vertically averaged velocity components, p the pressure, h the water depth and τ_{sy} and τ_{by} are surface and bottom stresses in the alongshore direction (e.g., Brink, 1997). The presence of coastally trapped waves is indicated by the tendency for the first three terms in this equation to balance. In cases such as off Peru (Allen and Smith, 1981), where the waves behave nearly as Kelvin waves, the alongshore acceleration and pressure gradient alone tend to balance.

In general, coastal-trapped wave properties observed at a particular location depend on the earth's rotation, the density stratification in the water column and the bottom slope. The essential dynamics involve vorticity conservation: the relative vorticity (tendency to spin) of a portion of the water column changes as the height of a segment of water column stretches or contracts. Thus, either changes in the vertical separation between density surfaces or variations in total water depth for a barotropic flow can excite relative vorticity, hence changes in alongshore flow. In either case, the wave motions tend to decay away from the shelf–slope boundary, and the sense of wave phase propagation is always such that the coast is on the right, viewed facing the direction of wave propagation in the Northern Hemisphere and in the opposite direction in the Southern Hemisphere. The relative importance of stratification versus bottom slope for coastally trapped waves can be measured by the Burger number (e.g., Huthnance, 1978),

$$S = \frac{N^2H^2}{f^2L^2} \tag{2}$$

where N^2 is a typical buoyancy frequency squared (a measure of the density stratification), H a representative depth of the ocean offshore of the shelf and slope, f the Coriolis parameter and L the total width of the shelf–slope topography. When S is large, as can happen at low latitudes, the waves behave essentially as internal Kelvin waves (e.g., Gill and Clarke, 1974), and the cross-shelf flow in equation 1 is unimportant. When S is small, as often happens over wide continental margins away from the tropics, flow tends to be depth independent, at least over the shelf, and stratification can be ignored: this is the barotropic continental shelf-wave limit (e.g., Gill and Schumann, 1974). There has been an historical tendency to make distinctions between Kelvin and shelf waves, but this has been caused largely by the need for simplification to gain analytical solutions rather than because there is a substantial dynamical difference.

Coastally trapped waves are generated by winds and tides and as a result of eastward-propagating equatorially trapped Kelvin waves, which impinge on the eastern boundary and are then deflected to propagate poleward along the coastal waveguide. Coastally trapped waves are efficiently generated by the alongshore component of wind stress (Huthnance, 1981; Gill, 1992), so that the effects of winds at a given location are felt as currents, with a time delay, at a range of locations alongshore. When the winds cause an upward bulge of the thermocline through upwelling, this bulge can, in principle, propagate similarly alongshore. The wider significance of CTWs is that they are a mechanism by which, in principle, upwelling signatures could be propagated to remote locations, although there are few, if any, direct observations of this. However, the mechanism is thought to be relevant off Equatorial West Africa, where coastal upwelling does not appear to be related to the local wind forcing, and an explanation in terms of propagating waves has been sought (Chapter 21).

Off the west coasts of North and South America, coastally trapped waves with characteristic phase speeds of 2–4 m s^{-1} have been observed. These are revealed by the pronounced sea-level signatures (amplitude 0.1–1 m) that accompany them. Off the west coast of North America (Chapter 12) and several other regions, CTWs are quasibarotropic in character at the important time scales (3–10 days) with no evidence of pycnocline displacements. Off Peru, observed waves are characteristic of first-mode baroclinic CTWs, some of which probably originate in the equatorial region, although further poleward toward midlatitude Chile, the coherence between the wind and sea level increases, indicating the increasingly important role of locally (several 100 km equatoward) generated CTWs. Off the west coast of North America, waves on time scales of 2–10 days are driven by coastal alongshore winds, and equatorial influences appear to occur only at much longer time scales. Propagating waves with a longer period (20–30 days), unrelated to local winds, have been observed in the Southern California Bight (Hickey, 1992). CTWs have been observed to propagate anticlockwise around southern Africa. Speeds have been deduced from tide gauge records of sea level and appear to increase from the west coast (2–3 m s^{-1}) to the south coast (5 m s^{-1}). CTWs propagate only infrequently northward (equatorward) on the east coast of South Africa because of interference by the Agulhas Current (Chapter 19).

Tides can be responsible for the generation of continental shelf waves (e.g., Pingree and Griffiths, 1984). A diurnal period nondivergent shelf wave propagates northward along the Hebridean shelf west of Britian and is manifest by enhanced diurnal period tidal currents with no corresponding diurnal signal in the predominantly semidiurnal elevation signal (Cartwright, 1969; Cartwright et al., 1980). Trapped diurnal waves are also predicted over the offshore banks west of Britain (Pingree and Griffiths, 1984) and a diurnal shelf wave is found on the Vancouver Island shelf forced at the mouth of the Juan de Fuca Strait (Thomson and Crawford, 1982; Flather, 1988).

On the northern Gulf of Guinea coast, Ajao and Houghton (Chapter 21) comment on the presence of CTWs in several period bands, but a prominent wave, which propagates with a speed of 0.42 m s^{-1}, has a period of 14.77 days (the MS_f tidal period). This wave is possibly generated through nonlinear interaction of the M_2 and S_2 tidal constituents on the broad shelf off the Niger River Delta (Chapter 21).

3.5. *Fronts*

Fronts are ubiquitous features on eastern boundaries, and several types of front that already have been mentioned (upwelling, plume and coastal current fronts) are not discussed further. At several locations along eastern boundaries, major oceanic water mass fronts are found which tend to be oriented zonally with respect to the meridional coastline. These fronts are established by the confluence of water masses brought about by the offshore oceanic circulation. Notable examples are the NACW/SACW water mass front off northwest Africa (Chapter 22), the Equatorial Front (Chapter 10) and the Angola Front (Chapter 20).

Shelf-break fronts separating shelf waters from slope and oceanic waters (such as found on the U.S. Middle Atlantic Bight) are not particularly notable on eastern boundaries. The MAB front is primarily a haline feature separating fresher shelf water from more saline ocean waters, and the reduced runoff on eastern boundaries limits the scope for such fronts. Shelf-break thermal fronts can occur in upwelling systems, particularly if the upwelling front is locked to the shelf edge. The extensive northwest European shelf does not have a permanent shelf-break front, but a band of cold water observed in summer along the Celtic Sea shelf break is thought to result from enhanced shelf-break mixing due to dissipation of internal tide energy (Chapter 23; Pingree and Mardell, 1981).

On the extensive, tidally energetic eastern boundary shelves of northwest Europe and the Bering Sea, tidal mixing fronts are formed on a seasonal basis. These fronts separate waters that are permanently mixed from top to bottom by the tides from waters where there is insufficient tidally generated turbulence to prevent stratification in response to the input of surface buoyancy due to either heating (Europe) or the spring ice melt (Bering Sea). Tidal mixing fronts induce significant baroclinic circulations, which can be expected to constitute an important aspect of the seasonal circulation on these shelves (e.g., Chapter 23; Hill et al., 1997).

3.6. *Topographic Effects: Capes, Bays, Banks, Canyons and Islands*

The influence of topographic effects in the coastal ocean has been reviewed by Trowbridge et al. (1997). All eastern boundaries exhibit particular coastal features which can have important local impacts. The role of coastal promontories in triggering the instability of upwelling jets has already been noted. Although not all upwelling filaments are associated with promontories, where there is consistency in filament location a coastal feature is usually implicated, especially in the earlier stages of filament formation. Cape St. Vincent (Portugal), at the southern margin of the Iberian Upwelling system, is also associated with the generation of dipole eddy pairs visible in satellite infrared imagery. Capes and promontories are also involved in the promotion of localized or intensified coastal upwelling and thus introduce an important component of spatial variability into upwelling systems. Off South America, localized upwelling centers are particularly associated with capes bounding equatorward facing bays (Chapter 10).

Coastal embayments such as the Southern California Bight or Prince William Sound (Alaska) are occasionally associated with permanent gyre circulations [e.g., the cyclonic Southern California Eddy (Hickey, 1979)]. Other permanent gyres (usually cyclonic) associated with eastern boundaries are the Angola Dome and the Costa Rica Dome, although these are probably brought about by oceanic conditions rather than coastal topography (e.g., Chapter 11). The North Pacific eastern margin is traversed by a number of deep "sea valleys" of glacial origin. Consequently, in places the shelf is broken into a series of banklike features. The sea valleys may play an important role in causing the Alaskan Coastal Current to meander, thereby inducing offshore squirts. In a number of places on the Alaskan Shelf, semipermanent eddies or gyres like the anticyclonic Kayak eddy are formed over banklike topographic features. Off northwest Europe, offshore banks such as Porcupine Bank, Rockall Bank and Faeroe Bank are associated with quasipermanent (anticyclonic) circulations (Chapter 25). Tidal rectification around these banks can also induce closed around-bank flows (e.g., Huthnance, 1973; Loder, 1980; Pingree and Maddock, 1985). On the Northwest European Shelf, regions of weakened tidal stirring (often associated with topographic depressions) lead to the trapping of cold (dense), static bodies of water beneath the thermocline after the onset of summer stratification. These cold pools are separated from adjacent waters by bottom fronts which drive a seasonal, cyclonic near-surface circulation around the bottom water pool (Hill et al., 1997).

Canyons that intersect the continental slope can have a number of important influences and can modify the local circulation (Hickey, 1996, 1977). Dynamically, their most important effect is to allow the geostrophic constraint on steep slopes to be broken locally, thereby permitting increased cross-slope motion. They are also possible sites for dense water cascades to flow down the continental slope from the shelf (Huthnance, 1995) and intensified upwelling (typically, on their equatorward side). Internal tide motions (see later) can also be enhanced in canyons. Aside from the individual localized impacts of coastal and bathymetric irregularities, the form drag they induce is likely to play an important role in the rectification of subinertial motions and hence upon the dynamics of large-scale poleward flows on eastern boundaries (Holloway et al., 1989). Topographic irregularities such as ridges are also responsible for the scattering of coastally trapped waves (e.g., Chapter 12).

At some eastern boundary locations (e.g., California; Oey, 1996) offshore islands are located within the coastal transition zone. One of the most intensively studied cases is that of the Canaries Archipelago off northwest Africa (Chapter 22). The islands are located in the offshore Canary Current, which flows equatorward through the island group. Several effects are observed, including the generation of cyclonic eddies southwest of Gran Canaria and an apparently quasipermanent anticyclonic eddy south of the island of Tenerife. These eddies contribute to the mesoscale activity downstream. The islands are also located within the northeast trade wind belt (wind speed 5–10 m s^{-1}), and the intense wind shear that occurs between the wind shadow zone in the lee of an island and the main airstream that flows on either side of the islands can induce pronounced, localized Ekman pumping. The Canaries Archipelago is located sufficiently close to the northwest African coast that upwelling filaments extending from the coast intermittently "waft" through the island group, causing a marked drop in surface water temperatures. A similar process occurs in the Southern

California Bight, with water upwelled near Point Conception advected shoreward between many of the Channel Islands (Hickey, 1992).

Offshore wind jets associated with airflow through mountain passes are a topographically controlled phenomenon that is important in the Gulfs of Panama, Papagayo and Tehuantepec in Central America. These wind jets occur in winter and have durations of 3–4 days, attaining speeds greater than 20 m s^{-1}. The response in the ocean is marked cooling of surface waters by up to 8°C beneath the wind jet. The pronounced wind shear on either side of the wind jet induces pycnocline tilt due to Ekman pumping and suction on either side of the wind jet and results in an offshore "squirt" with velocities above 1 m s^{-1}. The surface cooling is due partly to upwelling brought about by the Ekman pumping and partly to wind mixing (Barton et al., 1993). The offshore squirt results in the spin-up of an anticyclonic eddy on the poleward side of the jet which propagates offshore into the ocean and contributes to the mesoscale eddy activity of the region. At the head of the gulf the offshore squirt produces a flow divergence that induces upwelling, a drop in coastal sea level and convergent coastal currents.

3.7. Internal Tide Generation

Internal tide generation occurs when the barotropic tide interacts with a sloping bottom in the presence of stratification. Internal tide energy is concentrated along ray characteristics of slope $[(\omega^2 - f^2)/(N^2 - \omega^2)]^{1/2}$, often resulting in bottom trapping of semidiurnal periodicities over critical slopes. Internal tides are not confined solely to eastern boundaries, but some of the most extensive studies of them have been made on eastern boundaries. Regions where they are known to be important include the Northwest Australian Shelf edge (Holloway, 1994), the Pacific west coast (Torgrimson and Hickey, 1979; Rosenfeld, 1990; Drakopoulas and Marsden, 1993), the Iberian Margin, the Strait of Gibraltar (e.g., Bryden et al., 1994), northwest Africa (Gordon, 1978; Huthnance and Baines, 1982); the Bay of Biscay and Celtic Shelf edge (Pingree and Mardell, 1981; New and Pingree, 1992; Chapter 23) and the Malin Hebrides Shelf (Sherwin, 1988). The role of internal tides at the shelf edge has been discussed more fully in a review by Huthnance (1995). The principal importance of internal tides concerns their contribution to diapycnal mixing at the ocean margin, particularly at critical locations where velocities are intensified at locations where the bottom slope matches the ray characteristic slope. Internal tide energy can also propagate from generation regions on the slope to be dissipated and bring about mixing on the shelf.

4. Discussion

The sections above, together with Table I, have demonstrated some of the commonality between eastern boundary phenomena and have provided a physically based account of some of the important processes that govern them. In this section we consider some of the outstanding scientific questions and goals for future research.

A general conceptual framework for the discussion of coastal circulation is provided by the distinction between local and remote forcing. In the context of the large-scale boundary currents discussed here, *local forcing* is that which occurs directly at the site of interest, although we extend the definition to include buoyancy forcing and wind stress, integrated over several hundred kilometers equatorward of the location of interest (i.e., the scale of wind systems). This includes some coastally trapped waves in the local forcing category. Although the winds several hundred kilometers away might be considered as distant, these are nevertheless the winds that would be used to predict local currents from long-wave models, incorporating the poleward-propagating characteristics of the coastal ocean. *Remote forcing* includes large-scale currents and poleward-propagating signals that affect the coastal ocean from outside the domain of the local winds. This dichotomy of local and remote forcing can be applied to the issues of interannual variability, shelf–ocean exchange and the mechanisms that drive poleward flow over the shelf, slope and farther offshore. All of these are considered in turn below.

A picture of the local wind forcing in each of the major eastern boundaries is provided by the annual cycle of alongshore wind stress as a function of latitude and month, presented in Fig. 2.7. These wind stress values are computed from the ECMWF (European Centre for Medium Range Weather Forcasting) wind fields, interpolated to locations 50 km offshore and resolved in the alongshore direction using the coastline orientation. Although these wind stress fields do not capture small-scale features of the wind field, they do allow an overview of the large-scale similarities and differences between the systems.

A well-known aspect of the wind forcing evident in Figure 2.7 is the difference in timing of maximum upwelling-favorable winds at midlatitude (maxima in spring and summer), compared to low latitude (upwelling favorable all year at lowest latitudes with maxima in winter and early spring). A more significant difference between the systems is the maximum values and areal extent and duration of those maxima. As described above, the wind-driven coastal circulation can be calculated with long-wave models, integrating the response along the coast equatorward from the location of interest. Thus the alongshore extent of wind forcing directly affects the circulation. In this respect, the coast of northwest Africa appears to be the most strongly forced, while the region off the Iberian peninsula appears to experience the weakest forcing. Wind stress appears similar in the California and Benguela Current systems and somewhat weaker and of lesser latitudinal extent off Chile. We also note that in all except the Benguela, there is a region of weaker upwelling between areas with stronger upwelling (the Southern California Bight, the region off southern Peru–northern Chile, the area around the Mediterranean outflow). These may have biological importance as areas with less turbulent mixing, favored for spawning by some species of fish (Lasker, 1981). The two strongest differences evident in these climatological means (Fig. 2.7) are a relatively reduced amplitude of the seasonal cycle of upwelling-favorable conditions at lowest latitudes in both the Southern Hemisphere eastern boundary current regions in comparison with their Northern Hemisphere counterparts and the relatively low latitudes to which the winter reversal to mean downwelling conditions extends along the Chilean coast.

The coastal sea-surface-temperature deficit presents a satellite measured estimate of coastal upwelling intensity (Fig. 2.7). Although biased both by offshore temperature variability, which departs from a strictly solar-forced seasonal cycle, and geographic regions with missing data close to the coast (high latitudes along the Chilean and South African coasts), these data show similar patterns in three of the boundary current regions in which seasonal cycles appear related to wind forcing over most latitudes. In both the California and Canary Currents, a strong deficit occurs at the

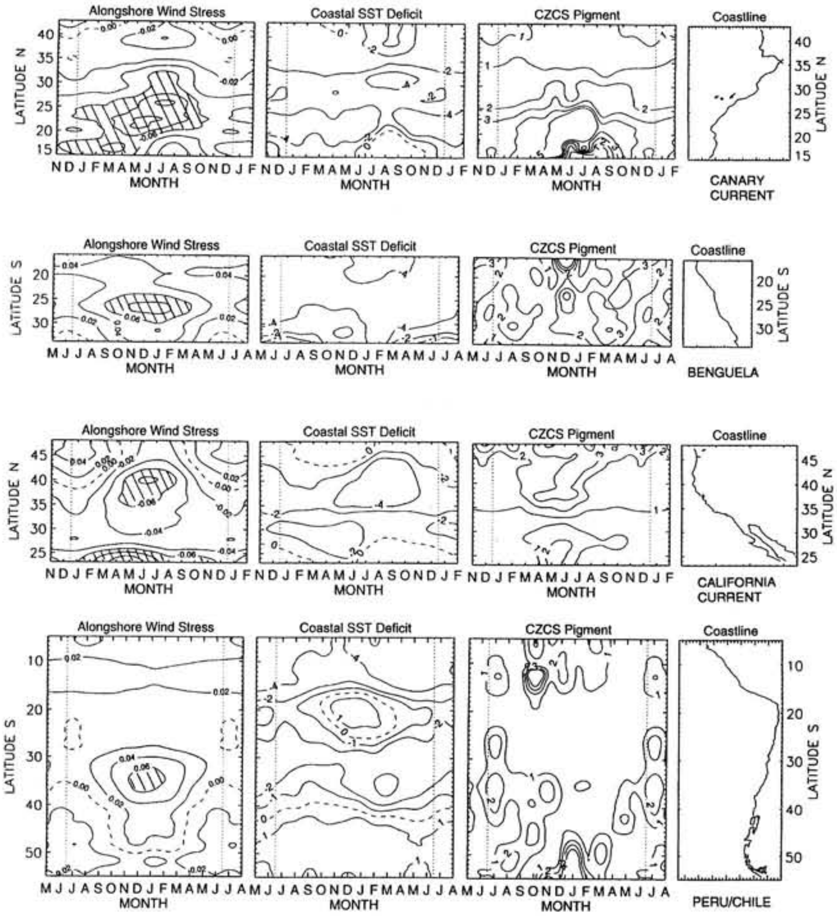

Fig. 2.7. Climatological seasonal cycles of the alongshore component of wind stress (N m^{-2}), coastal sea-surface temperature deficit (°C) and near-surface phytoplankton pigment concentrations (mg m^{-3}) plotted as a function of latitude in each of the four major eastern boundary currents. To facilitate comparison between hemispheres, months have been ordered such that summer is in the center of each plot. Alongshore wind stress is calculated from daily ECMWF fields interpolated to a position 50 km offshore and averaged by calendar month over the time period of the coastal zone color scanner mission (1979–1986). Northward wind stress is positive, making upwelling-favorable winds (equatorward winds) negative in the Northern Hemisphere and positive in the Southern Hemisphere. The coastal sea-surface temperature deficit is an indication of upwelling intensity. Temperatures are derived from satellite (NOAA AVHRR)-measured temperature fields for the period 1981–1986, composited into calendar months and calculated in each month as the difference between the closest available measurement to the coast and the mean temperature within a 100-km-wide region centered 1500 km offshore at the same latitude. Relatively cold coastal surface temperatures are negative. Phytoplankton pigment concentrations are derived from satellite (coastal zone color scanner)-measured pigment fields composited into calendar months over the lifetime of the mission (1979–1986). These fields were further composited spatially into 100 × 100 km bins oriented along the coast. Missing data still present in the CZCS time series after this temporal/spatial compositing (at the highest latitudes in the Peru–Chile Current and at lowest latitudes in the Canary Current) were filled by first latitudinal averaging of data within the same month and then temporal averaging of adjacent months at the same latitude. Both the AVHRR SST and the CZCS pigment fields are from climatological data sets prepared and released by NASA Jet Propulsion Laboratory, Physical Oceanography Distributed Active Archive Center.

latitudes of maximum upwelling-favorable winds. At the lowest latitudes this seasonality is temporally coincident with that of wind forcing, while at higher latitudes the maximum deficit follows the maximum in upwelling-favorable winds by one to two months. In both currents, there is a midlatitude region (23°N in the Canary Current and 30°N in the California Current) of reduced seasonal amplitude actually having a minimum in middle to late summer. These spatial and temporal patterns are repeated in the Benguela Current except at the lowest latitudes, where a slight minimum is present in summer. Patterns of coastal temperature deficit in the Peru–Chile Current are quite dissimilar to those in the other eastern boundary currents. Maximum deficits are present along the Peruvian coast, where upwelling-favorable winds are present throughout the year. Maximum seasonal variability in temperature deficit, however, occurs at midlatitudes where the seasonal variability in large-scale wind forcing is minimal. In this region (centered at 20°S), the seasonality of temperature deficit is opposite to that expected due to any seasonal upwelling but positively correlated to the seasonal cycle in solar heating. There is little seasonality at latitudes greater than 40°S, despite the seasonality evident in wind forcing. Only in a relatively narrow latitudinal zone (35 to 40°S) along the Chilean coast does the seasonality of coastal temperature deficit show minimum values in late summer, lagging maximum wind forcing by one to two months and resembling patterns evident in the other eastern boundary currents.

As with local wind forcing, each eastern boundary current demonstrates qualitative similarities in their interaction with basin-scale currents, but details are different in each case. With respect to low-latitude distant forcing, equatorial currents appear to impinge directly on two eastern boundaries. The Pacific equatorial undercurrent is thought to feed into the poleward undercurrent and Peru–Chile Countercurrent off Peru (Chapter 10). In the Atlantic, the North Equatorial Countercurrent feeds the flow along the coast of northwest Africa to Cap Blanc (20°N) (Chapter 22). Off Peru, northern Chile and the low-latitude part of northwest Africa, these offshore poleward currents represent a lateral stress that causes onshore transport, through the earth's rotation, opposing offshore Ekman transport driven by equatorial winds. The poleward currents appear to be maximum when equatorward winds are minimum, in local spring and summer. A similar poleward flow appears to occur in the low-latitude eastern South Atlantic, but details of that circulation are not well studied. The interaction between the upwelling systems, winds and the poleward offshore currents remains an unexplored area.

In the regions between low and midlatitudes, three of the systems change from equatorward flow at midlatitudes to westward flow in a region of confluence with the poleward, low-latitude currents described above. The California Current turns offshore near the Costa Rica Dome (10°N), the Benguela Current turns offshore near the Angola Dome (15°S) and the Canary Current turns offshore near Cap Blanc (20°N). Only the Peru–Chile Current seems to flow fairly continuously to the equator, where it turns westward into the South Equatorial Current. The reason for this difference off South America is not clear and represents another open question.

The cause of interannual and decadal-scale variability is an important issue that concerns eastern boundaries. The most striking form of interannual variability is the El Niño–Southern Oscillation cycle, which affects the Pacific margin and distinguishes it markedly from other eastern boundaries. During El Niño events there is temporary strengthening of the poleward current, deepening of the thermocline, southward shift in the ITCZ (which brings heavy rain to normally arid regions), weakening of the subtropical anticyclone and equatorward shift of the region affected by coastal atmospheric lows. Contrary to what might be expected, there is little reduction in upwelling-favorable winds during El Niño events (Chapter 10) but since the nutricline is also depressed, upwelling supplies a reduced level of new nitrogen to the coastal ecosystem.

Interannual variability can be examined as a combination of local and remote forcing. In the Pacific the remote forcing arrives as poleward-propagating features from El Niño events along the California and Peru–northern Chile coast. The local forcing is also affected by the equatorial region, transmitted through the atmosphere Hadley and Walker cells, atmospheric pressure systems, then coastal winds). Changes in storm paths during the 1982–1983 El Niño increased winter storms, onshore Ekman transport, coastal temperatures and sea levels. The extent to which the coastal ocean response during El Niños is due to relatively local atmospheric forcing (e.g., winds or heat flux) or to oceanic connections to the equatorial region is an area open for further research.

Aside from El Niño cycle, in the North Pacific there is evidence of a 15- to 20-year cycle in atmospheric and shelf bottom water temperatures, possibly related to the 18.6-year lunar nodal tide (Chapter 13). In basins other than the Pacific, the causes of interannual or decadal-scale variability are less clear and long time series are rare. The evidence for "Atlantic El Niños" remains inconclusive, although there clearly are nonlocal influences across the Equatorial Atlantic because the appearance of cold upwelled water in the Gulf of Guinea appears to be related to winds in the Western Equatorial Atlantic (Chapter 21). The closest to an Atlantic equivalent of Pacific El Niños is probably the Benguela Niños of the South Atlantic, but their mechanism remains unexplained (Chapter 20). Are they tied to ENSO through atmospheric teleconnections, or are they driven by a separate Atlantic oscillator? The North Atlantic Oscillation, a measure of the atmospheric pressure difference between the Azores High and the Southeast Iceland Low has been related to fluctuations of fish stocks in the North Atlantic (Cushing, 1995) and may also be implicated in the interannual cycle of precipitation over northwest Africa known locally as "Al Mubarak." The Great Salinity Anomaly (Dickson et al., 1988), a general freshening of the upper 500–800 m of the northern North Atlantic, has also been a major decadal-scale oceanic signal which has not been fully explained. The low-salinity anomaly was traced cyclonically around the northern North Atlantic over 14 years and on the eastern boundary was manifest by a negative salinity anomaly of up to 0.3 off the northwest European continental shelf during the mid-1970s. The pattern of exchange of ocean water with the shelf in the northern North Sea may have been influenced by these salinity changes during the Great Anomaly (Turrell, 1992). In the northwest Africa region reports from various sites indicate that upwelling intensity (as indicated by the upwelling index or sea-surface temperature anomaly) increased substantially from the 1960s to 1970s and has decreased again through the 1980s (Chapter 22). The circulation of a large cool feature around the North Atlantic subtropical gyre reported by Hansen and Bezdek (1996) is compatible with these interpretations. The relation of the cool anomaly to the Great Salinity Anomaly is not yet clear, although it may be anticipated that there is one. Since 1940, downwelling has increased in winter off the northern part of the west coast of north America, but upwelling has increased off Baja California. On the other hand, summertime upwelling has increased off much of the west coast over this period (Hseih et al., 1995). On the global scale Bakun (1990) deduced that there has been an overall increase in upwelling intensity, possibly due to enhancement of the large-scale pressure contrasts driving the trade winds. Clearly, much more needs to be done to identify the causes of interannual variability in the oceans and to assess their impact on eastern boundary systems. In this regard, the maintenance of long time series is clearly of great importance, and the CalCOFi time series on the U.S. west coast dating back to the 1950s have, for instance, played an important role in our present understanding of El Niño and related events.

A full discussion of the impacts of eastern boundary processes on marine ecosystems is beyond the scope of this chapter, but accounts can be found in the books by Cushing (1995) and Mann and Lazier (1991). The large vertical velocities in coastal upwelling systems supply nutrients to the photic zone and thus stimulate primary production. In eastern boundary systems the large-scale lateral advection can also supply nutrients (e.g., equatorward flows from the nutrient-rich subarctic water in the northern Pacific; Roesler and Chelton, 1987). High concentrations of chlorophyll pigments in coastal upwelling systems are plainly evident in satellite, sea-color imagery (Shannon, 1985; Strub et al., 1990; van Camp et al., 1991; Thomas et al., 1994). Phytoplankton pigment concentrations (Fig. 2.7) represent an estimate of the biological response to the upwelling of nutrient-rich water. In Fig. 2.7 the CZCS data coverage is most complete for the two Northern Hemisphere regions. Seasonal cycles of pigment concentration in both the California and Canary Currents show highest concentrations during summer months at most latitudes, coincident with the seasonal maximum upwelling-favorable winds. In each region, there is a seasonal northward progression of elevated pigment concentrations associated with the seasonal northward progression of upwelling-favorable winds. In both of these current regions there is a latitudinal zone exhibiting little pigment concentration seasonality despite strong wind forcing seasonality. In each case this region is associated with strong changes in coastal orientation (the California Bight at 34°N and the Gulf of Cadiz–Strait of Gibraltar at 35°N). A reduced number of available satellite measurements coupled with missing data in both Southern Hemisphere regions means that these seasonal cycles must be treated with caution. In the Benguela Current, maximum concentrations are evident in summer extending over lower and middle latitudes. At the highest latitudes, maximum concentrations occur in late summer. Patterns evident in these satellite data in the Peru–Chile Current suggest seasonality quite different from that in the other eastern boundary currents. At the lowest latitudes where the seasonality in wind forcing is minimal, seasonality in pigment concentrations is relatively strong with maximum concentrations occurring in summer. At midlatitudes (20–40°S), the seasonal variability evident suggests that minimum concentrations occur in summer, associated with the maximum in upwelling-favorable winds. At the highest latitudes, the maximum in pigment concentration occurs in summer but is associated with mean downwelling-favorable winds. In this region, strongly variable winds due to storms and the complex coastline orientation reduce the significance of monthly averaged wind vectors.

The biological response to upwelling is complex in that it is affected by a variety of feedback mechanisms within the ecosystem (e.g., Cushing, 1995). Despite similar physical characteristics, the fisheries productivity of upwelling systems differs between the South American fisheries (more productive than those on any other eastern boundary) and those of other upwelling regions. This raises important questions about the differences in ecosystem structure in the various upwelling systems (Chapter 10). Cury and Roy (1989) relate the recruitment of the Pacific sardine to water column turbulence taken as proportional to the cube of the wind speed. Recruitment depends on turbulence in a dome-shaped manner above wind speeds of 5–6 m s^{-1} (increasing turbulence is likely to mix phytoplankton cells to depths below the photic zone, thus reducing primary production and the sardine food supply). Cury and Roy argue that there is an environmental window within which sardines are able to survive. Their argument has also been extended to other upwelling areas and to different species, with much the same result (Cushing, 1995). An increase in wind strength in response to global warming, say, could thus have major implications for fisheries recruitment in upwelling regions if the effect is to push these systems outside the environmental window.

Upwelling systems affect higher trophic levels not only through food chain–mediated processes (primary production), but the current systems may offer opportunities for transport of zooplankton prey and fish larvae to nursery areas (e.g., Sinclair, 1988). For example, vertical migratory behavior in relation to the vertical shear in both alongshore and cross-shore currents could enable organisms to regulate their horizontal position (e.g., Peterson et al., 1979).

Our understanding of the biological response to upwelling and tidal mixing systems is fairly well developed, but further progress is needed in relation to buoyancy-driven systems. Although our understanding of ecosystem changes in relation to El Niño events off Peru is reasonably good (e.g., Barber et al., 1985), in other regions, such as the northwest Pacific, major fluctuations in economically important species such as salmon, herring and hake occur over years to decades. Present management indices for these species are based on correlations with convenient proxy environmental variables. However, the aim is to obtain leading indices for these changes which give some degree of prognostic capability. Such a goal will inevitably require greater understanding of the underlying physical and biological mechanisms and their interactions. This, however, raises a fundamental question as to the limits of biological predictability. If we had a perfect prediction capability for physics, what would it buy biologically, and how good would the biological model or observation system have to be to reach a given level of skill? The key to understanding the impact of physics on marine ecosystems and, in particular, on economically important species lies with the marine zooplankton, which occupy a pivotal role in the food web. Zooplankton production is affected by physics not only through its control on primary production, but also through the direct influence of physics on zooplankton feeding rates (as affected by the ambient turbulence field) as well as through large-scale advection–diffusion processes which affect the relative distribution of predator and prey. Many of these complex issues are the subject of various national and international GLOBEC programs, including (1) the impact of fluctuations in the physical environment (including due to climate change) on zooplankton and the larvae of economically important species, and (2) the development of appropriate-scale coupled physical–biological models.

An important general issue concerning the ocean margins is the extent of shelf–ocean exchange. Tracers such as ^{18}O are useful for obtaining volumes and rates of exchange but tell us nothing of the mechanisms. The topic of shelf-edge exchange has recently been reviewed by Huthnance (1995), who estimated the cross-shelf exchange for a variety of individual processes known to occur at the ocean margin. On eastern boundaries the processes associated with shelf–ocean exchange include the onshore–offshore Ekman upwelling circulations (e.g., concentrated in canyons), upwelling filaments and squirts, and baroclinic coastal current eddies. The poleward slope current will also induce downslope bottom Ekman layer drainage where it impinges on the slope. Separation from the coastal boundary of the major ocean current systems may also draw eastern boundary water offshore. Examples are to be found off southwest Africa (associated with the Angola Front) and off northwest Africa (associated with the Cabo Blanco giant filament), where the oceanic subtropical gyre flows separate from the coastal margin. Huthnance (1995) found a characterstic exchange value on the order of 1 Sv per 1000 km (1 Sv = 10^6 m^3 s^{-1}) for each of the major processes (equivalent to an upwelling index of 100). The estimates must be treated with some caution, however. For example, the net water fluxes (i.e., taking into account possible on-shelf return flow) associated with upwelling filaments are uncertain. Filaments, of course, are possibly implicated in a different form of shelf–ocean exchange because the offshore jet carries cold, rich, upwelled water far offshore over the deep ocean. While the jet may meander back near the coast, subduction and biological activity along the path of the jet alter the chemical and biological properties of water in the jet and probably contribute to the biological pump by the rain of material to the deep-ocean sediments in the 500 km next to the coast. For the eastern boundary it is likely that exchanges, often related to upwelling, are more effective than in many other ocean margin regions.

The distinction between remote and local forcing is again relevant when considering shelf-edge exchanges. For example, a filament, formed by instability of the equatorward-flowing upwelling-front jet (perhaps initiated at a coastal promontory), appears to begin as a locally forced phenomenon but eventually affects the large-scale deep ocean. In contrast, the large filaments in the Benguela system are brought about by a different mechanism, interaction with Agulhas rings. Hence the shelf-edge exchange brought about by ring-induced filaments is ultimately forced by the remote processes involved in ring generation.

The poleward-flowing undercurrent or slope current is a ubiquitous phenomenon, although the extent to which the observed fragments of poleward flow on eastern boundaries are actually part of a continuous current system remains unclear. The existence of poleward flow ought to provide a unifying dynamical framework for eastern boundaries, but the mechanism that drives the poleward flow also remains uncertain. Large-scale oceanically imposed meridional pressure gradients, rectification of subinertial motions through form stress and wind are the main contenders. In particular, more attention should be paid to form stress models, especially those that include realistic stratification. Such models should provide more symptoms of form-stress-driven boundary currents to test against the observations. Statistically, however, the problem in testing these models is that each mean flow has only one degree of freedom, so that the usual tests applicable to fluctuating currents are of no value. Testing of models against data thus relies on comparison of model flow fields with spatially distributed mean flow observations, and the latter are difficult to obtain. Moreover, the reliability of models is limited by the quality of inputs (forcing functions) and parameterizations (e.g., lateral or vertical mixing).

We have now reached the point where a good first-order understanding of a number of individual eastern boundary processes has been obtained. Can we understand the physical system merely by linear superposition of individual responses, or are there complex nonlinear interactions that remain to be explored? A particular challenge for the future is incorporation of sediments and other particulates, chemistry and biology into models of eastern boundary systems, and these will certainly introduce nonlinearities into the coupling process. To test such models, future programs will increasingly rely on an integrated, multidisciplinary approach to observations on eastern boundaries. From a management point of view, a sound scientific understanding of eastern boundary regions is increasingly important and we can expect that this will ultimately be expressed through a predictive capability for both natural and anthropogenic changes using models. The hope is that improved understanding will contribute toward rational management approaches and so mitigate overexploitation and perhaps avoid future conflict as pressure on resources mounts over the next century.

References

Allen, J. S., 1980. Models of wind-driven currents on the continental shelf. *Annu. Rev. Fluid Mech.*, **12,** 389–433.

Allen, J. S. and R. L. Smith, 1981. On the dynamics of wind-driven shelf currents. *Philos. Trans. R. Soc. London Ser. A*, **302,** 617–634.

Bakun, A., 1990. Global climate change and intensification of coastal upwelling. *Science*, **247,** 198–201.

Barber, R. T., F. P. Chavez, and J. E. Kogelschatz, 1985. Biological effects of El Niño. In *Seminario Regional Ciencas Tecnología y Agresión Ambiental: El Fenómeno "El Niño,"* M. Vegas, ed. Contec Press, Lima, Peru, pp. 399–438.

Barton, E. D., M. L. Argote, J. Brown, P. M. Kosro, M. F. Lavin, J. M. Robles, R. L. Smith, A. Trasviña and H. S. Velez, 1993. Supersquirt: dynamics of the Gulf of Tehuantepec, Mexico. *Oceanography*, **6,** 23–30.

Battisti, D. S. and B. M. Hickey, 1984. Application of remote wind forced coastal trapped wave theory to the Oregon and Washington coasts. *J. Phys. Oceanogr.*, **14,** 887–903.

Brink, K. H., 1991. Coastal trapped waves and wind-driven currents over the continental shelf. *Annu. Rev. Fluid Mech.*, **23,** 389–412.

Brink, K. H., 1997. Wind-driven currents over the continental shelf. In *The Sea*, Vol. 10, *The Global Coastal Ocean: Processes and Methods*, K. H. Brink and A. R. Robinson, eds. Wiley, New York, Chap. 1.

Brink, K. H. and T. J. Cowles, 1991. The coastal transition zone programme. *J. Geophys. Res.*, **96,** 14637–14647.

Bryden, H. L., J. Candela and T. H. Kinder, 1994. Exchange through the Strait of Gibraltar. *Prog. Oceanogr.*, **33,** 201–248.

Cartwright, D. E., 1969. Extraordinary tidal currents near St. Kilda. *Nature (London)*, **223,** 928–932.

Cartwright, D. E., J. M. Huthnance, R. Spencer and J. M. Vassie, 1980. On the St. Kilda shelf tidal regime. *Deep-Sea Res.*, **27A,** 61–70.

Chapman, D. C. and R. C. Beardsley, 1989. On the origin of shelf water in the Middle Atlantic Bight. *J. Phys. Oceanogr.*, **19,** 384–391.

Csanady, G. T., 1978. The arrested topographic wave. *J. Phys. Oceanogr.*, **8,** 47–62.

Csanady, G. T., 1982. *Circulation in the Coastal Ocean*. D. Reidel, Dordrecht, The Netherlands.

Cury, P. and C. Roy, 1989. Optimal environmental window and pelagic fish recruitment success in upwelling areas. *Can. J. Fish. Aquat. Sci.*, **46,** 670–680.

Cushing, D. H., 1995. *Population Production and Regulation in the Sea: A Fisheries Perspective*. Cambridge University Press, Cambridge, 354 pp.

Denbo, D. W. and J. S. Allen, 1987. Large scale response to atmospheric forcing of shelf currents and coastal sea level off the west coast of North America: May–July 1981 and 1982. *J. Geophys. Res.*, **92,** 1757–1782.

DeSzoeke, R. A. and J. G. Richman, 1984. On wind-driven mixed layers with strong horizontal gradients: a theory with application to coastal upwelling. *J. Phys. Oceanogr.*, **14,** 364–377.

Dickson, R. R., J. Meincke, S.-A. Malmberg and A. J. Lee, 1988. The "Great Salinity Anomaly" in the northern North Atlantic. *Prog. Oceanogr.*, **20,** 103–151.

Drakopolous, P. G. and R. F. Marsden, 1993. The internal tide off the west coast of Vancouver Island. *J. Phys. Oceanogr.*, **23,** 758–775.

FAO, 1992. *Annual Report.* Food and Agriculture Organization, Rome.

Flament, P., L. Armi and L. Washburn, 1985. The evolving structure of an upwelling filament. *J. Geophys. Res.*, **90,** 11765–11778, 11835–11836.

Flather, R. A., 1988. A numerical model investigation of tides and diurnal period continental shelf waves along Vancouver Island. *J. Phys. Oceanogr.*, **18,** 115–139.

Gill, A. E., 1992. *Atmosphere–Ocean Dynamics.* Academic Press, San Diego, Calif.

Gill, A. E. and A. J. Clarke, 1974. Wind induced upwelling, coastal currents and sea level changes. *Deep-Sea Res.*, **21,** 325–345.

Gill, A. E., and E. H. Schumann, 1974. The generation of long shelf waves by the wind. *J. Phys. Oceanogr.*, **4,** 83–90.

Godfrey, J. S. and K. R. Ridgway, 1985. The large-scale environment of the poleward flowing Leeuwin Current, Western Australia: longshore steric height gradients, windstresses and geostrophic flow. *J. Phys. Oceanogr.*, **15,** 481–495.

Gordon, R. L., 1978. Internal wave climate near the coast of northwest Africa during JOINT-1. *Deep-Sea Res.*, **25,** 625–643.

Greenberg, D. A. and B. D. Petrie, 1988. The mean barotropic circulation on the Newfoundland shelf and slope. *J. Geophys. Res.*, **93,** 15541–15550.

Griffiths, R. W. and P. F. Linden, 1982. Laboratory experiments on fronts. 1. Density driven boundary currents. *Geophys. Astrophys. Fluid Dyn.*, **19,** 159–187.

Haidvogel, D. B. and K. H. Brink, 1986. Mean currents driven by topographic drag over the continental shelf and slope. *J. Phys. Oceanogr.*, **16,** 2159–2171.

Hansen, D. and H. F. Bezdek, 1996. On the nature of decadal anomalies in North Atlantic sea surface temperature. *J. Geophys. Res.*, **101,** 8749–8758.

Hart, H. J. and R. I. Currie, 1960. The Benguela Current. *Discovery Rep.*, **31,** 123–298.

Haynes, R., E. D. Barton and I. Pilling, 1993. Development, persistence and variability of upwelling filaments off the Atlantic coast of the Iberian Peninsula. *J. Geophys. Res.*, **98,** 22681–22692.

Hermann, A. J., B. M. Hickey, C. F. Mass, and M. D. Albright, 1990. Orographically trapped coastal wind events in the Pacific northwest and their oceanic response. *J. Geophys. Res.*, **95,** 13169–13193.

Hickey, B. M. 1979. The California Current system: hypotheses and facts. *Prog. Oceanogr.*, **8,** 191–279.

Hickey, B. M., 1992. Circulation over the Santa Monica–San Pedro basin and shelf. *Prog. Oceanogr.*, **30,** 37–115.

Hickey, B. M., 1996. Coastal submarine canyons. In *Proc. 'Aha Huliko'a Workshop on Flow Topography Interactions*, Honolulu, Hawaii.

Hickey, B. M., 1997. Response of a narrow submarine canyon to strong wind forcing. *J. Phys. Oceanogr.*, **27,** 679–726.

Hickey, B. M., R. E. Thomson, H. Yih and P. H. LeBlond, 1991. Velocity and temperature fluctuations in a buoyancy-driven coastal current off Vancouver Island. *J. Geophys. Res.*, **96,** 10507–10538.

Hickey, B. M., L. Pietrafesa, D. Jay and W. C. Boicourt, in press. The Columbia River Plume Study: subtidal variability of the velocity and salinity fields. *J. Geophys. Res.*.

Hill, A. E., 1997. Buoyancy effects in coastal and shelf seas. In *The Sea*, Vol. 10, *The Global Coastal Ocean: Processes and Methods*, K. H. Brink and A. R. Robinson, eds. Wiley, New York, Chap. 2.

Hill, A. E. and E. G. Mitchelson-Jacob, 1993. Observations of a poleward-flowing saline core on the continental slope west of Scotland. *Deep-Sea Res.*, **40,** 1521–1527.

Hill, A. E., J. Brown and L. Fernand, 1997. The summer gyre in the western Irish Sea: shelf sea paradigms and management implications. *Estuarine Coastal Shelf Sci.*, **44**(Suppl. A), 83–95.

Holloway, G., 1987. Systematic forcing of large-scale geophysical flows by eddy-topography interaction. *J. Fluid Mech.*, **184,** 463–476.

Holloway, P. E., 1994. Observations of internal tide propagation on the Australian northwest shelf. *J. Phys. Oceanogr.*, **24,** 1706–1716.

Holloway, G., K. H. Brink and D. Haidvogel, 1989. Topographic stress in coastal circulation dynamics. In *Poleward Flows Along Eastern Boundaries*, S. J. Neshyba, C. N. K. Mooers, R. L. Smith and R. T. Barber, eds. Springer-Verlag, New York, pp. 315–330.

Hsieh, W. W., D. M. Ware and R. E. Thomson, 1995. Wind-induced upwelling along the west coast of North America, 1899–1988. *Can. J. Fish. Aquat. Sci.*, **52,** 325–334.

Huthnance, J. M., 1973. Tidal current asymmetries over the Norfolk sandbanks. *Estuarine Coastal Mar. Sci.*, **1,** 89–99.

Huthnance, J. M., 1978. On coastal trapped waves: analysis and numerical calculation by inverse iteration. *J. Phys. Oceanogr.*, **8,** 74–92.

Huthnance, J. M., 1981. Waves and currents near the continental shelf edge. *Prog. Oceanogr.*, **10,** 193–226.

Huthnance, J. M., 1984. Slope currents and JEBAR. *J. Phys. Oceanogr.*, **14,** 795–810.

Huthnance, J. M., 1995. Circulation, exchange and water masses at the ocean margin: the role of physical processes at the shelf edge. *Prog. Oceanogr.*, **35,** 353–431.

Huthnance, J. M. and P. G. Baines, 1982. Tidal currents in the northwest African upwelling region. *Deep-Sea Res.*, **29,** 285–306.

Huyer, A., 1990. Shelf circulation. In *The Sea*, Vol. 9, *Ocean Engineering Science*, Part B, B. LeMehaute and D. M. Hanes, eds. Wiley, New York, pp. 423–466.

Huyer, A., E. J. Sobey and R. L. Smith, 1979. The spring transition in currents over the Oregon continental shelf. *J. Geophys. Res.*, **84,** 6995–7011.

Huyer, A., M. Knoll, T. Paluszkiewicz and R. L. Smith, 1991. Coastal upwelling off Peru during normal and El Niño times, 1981–1984. *J. Geophys. Res.*, **93,** 14297–14307.

Kelly, K. A. and D. C. Chapman, 1988. The response of stratified shelf and slope waters to steady offshore forcing. *J. Phys. Oceanogr.*, **18,** 906–925.

Kosro, P. M. and A. Huyer, 1986. CTD and velocity surveys of seaward jets off northern California, July 1981 and 1982. *J. Geophys. Res.*, **91,** 7680–7690.

Lasker, R., 1981. Factors contributing to the variable recruitment of the northern anchovy (*Egraulis mordax*) in the California Current: contrasting years 1975–1978. *Rapp. P.-V. Reun. Cons. Int. Explor. Mer*, **178,** 375–388.

Lentz, S. J., 1992. The surface boundary layer in coastal upwelling regions. *J. Phys. Oceanogr.*, **22,** 1517–1539.

Lentz, S. J., 1994. Current dynamics over the northern California inner shelf. *J. Phys. Oceanogr.*, **25,** 2461–2478.

Lentz, S. J. and J. H. Trowbridge, 1994. The bottom boundary layer over the northern California shelf. *J. Phys. Oceanogr.*, **24,** 1186–1201.

Loder, J. W., 1980. Topographic rectification of tidal current on the sides of Georges Bank. *J. Phys. Oceanogr.*, **10,** 1399–1416.

Mann, K. H. and J. R. N. Lazier, 1991. *Dynamics of Marine Ecosystems*. Blackwell, Boston, 466 pp.

McCreary, J. P., 1981. A linear stratified model of the coastal undercurrent. *Philos. Trans. R. Soc. London Ser. A*, **302,** 385–413.

McCreary, J. P., S. R. Shetye and P. K. Kundu, 1986. Thermohaline forcing of eastern boundary currents: with application to the circulation off the west coast of Australia. *J. Mar. Res.*, **44,** 71–92.

Münchow, A. and R. W. Garvine, 1993. Buoyancy and wind forcing of a coastal current. *J. Mar. Res.*, **51,** 293–322.

Neshyba, S., C. N. K. Mooers, R. L. Smith and R. T. Barber, 1989. *Poleward Flows Along Eastern Boundaries*. Springer-Verlag, New York.

New, A. L. and R. D. Pingree, 1992. Local generation of internal soliton packets in the central Bay of Biscay. *Deep-Sea Res.*, **39,** 1521–1534.

Oey, L.-Y., 1996. Flow around a coastal bend: a model of the Santa Barbara Channel eddy. *J. Geophys. Res.*, **101,** 16667–16682.

Peterson, W., C. B. Miller and A. Hutchinson, 1979. Zonation and maintenance of copepod populations in the Oregon upwelling zone. *Deep-Sea Res.*, **26,** 467–494.

Pingree, R. D. and D. K. Griffiths, 1984. Trapped diurnal waves on Porcupine and Rockall Bank. *J. Mar. Biol. Assoc. U.K.*, **64,** 889–897.

Pingree, R. D. and B. Le Cann, 1989. Celtic and Armorican slope and shelf residual currents. *Prog. Oceanogr.*, **23,** 303–338.

Pingree, R. D. and B. Le Cann, 1992. Three anticyclonic slope water oceanic eddies (SWODDIES) in the southern Bay of Biscay in 1990. *Deep-Sea Res.*, **39,** 1147–1175.

Pingree, R. D. and L. Maddock, 1985. Rotary currents and residual circulation around banks and islands. *Deep-Sea Res.*, **32,** 929–947.

Pingree, R. D. and G. T. Mardell, 1981. Slope turbulence, interval waves and phytoplankton growth at the Celtic Sea shelf break. *Philos. Trans. R. Soc. London Ser. A*, **302,** 663–682.

Roesler, C. and D. Chelton, 1987. Zooplankton variability in the California Current, 1951–1982. *CalCOFI Rep.*, **XXVIII.**

Rosenfeld, L. K., 1990. Baroclinic semidiurnal tidal currents over the continental shelf off northern California. *J. Geophys. Res.*, **95,** 22153–22172.

Shannon, L. V., ed., 1985. *South African Ocean Colour and Upwelling Experiment.* Sea Fisheries Research Institute, Cape Town, South Africa, 269 pp.

Sherwin, T. J., 1988. Analysis of an internal tide observed on the Malin Shelf north of Ireland. *J. Phys. Oceanogr.*, **18,** 1035–1050.

Sinclair, M., 1988. *Marine Populations: An Essay on Population Regulation and Speciation.* University of Washington Press, Seattle, Wash.

Strub, P. T., C. James, A. C. Thomas and M. R. Abbot, 1990. Seasonal and nonseasonal variability of satellite derived surface pigment concentrations in the California Current. *J. Geophys. Res.*, **95,** 11501–11530.

Thomas, A. C., F. Huang, P. T. Strub and C. James, 1994. Comparisons of the seasonal and interannual variability of phytoplankton pigment concentrations in the Peru and California Current systems. *J. Geophys. Res.*, **99,** 7355–7370.

Thomson, R. E. and W. Crawford, 1982. The generation of diurnal period shelf waves by tidal currents. *J. Phys. Oceanogr.*, **12,** 635–643.

Thomson, R. E., B. M. Hickey and P. H. LeBlond, 1990. The Vancouver Island Coastal Current: fisheries barrier and conduit. Effecs of ocean variability on recruitment and an evaluation of parameters used in stock assessment models. *Can. Spec. Pub. Fish. Aquat. Sci.*, **108,** 265–296.

Tomczak, M. and J. S. Godfrey, 1994. *Regional Oceanography: An Introduction.* Pergamon Press, Oxford.

Torgrimson, G. M. and B. M. Hickey, 1979. Barotropic and baroclinic tides over the continental slope and shelf off Oregon. *J. Phys. Oceanogr.*, **9,** 945–961.

Trowbridge, J. H., D. C. Chapman and J. Candela, 1997. Topographic effects, straits and the bottom boundary layer. In *The Sea*, Vol. 10, *The Global Coastal Ocean: Processes and Methods*, K. H. Brink and A. R. Robinson, eds. Wiley, New York, Chap. 3.

Turrell, W. R., 1992. New hypotheses concerning the circulation of the northern North Sea and its relation to North Sea fish stock recruitment. *ICES J. Mar. Sci.*, **49,** 107–123.

Van Camp, L. L. Nykjaer, E. Mittelstaedt and P. Schlittenhardt, 1991. Upwelling and boundary circulations off northwest Africa as depicted by infrared and visible satellite observations. *Prog. Oceanogr.*, **26,** 357–402.

Wang, D.-P., 1982. Effects of continental slope on mean shelf circulation. *J. Phys. Oceanogr.*, **12,** 1524–1526.